JVST B
Journal of Vacuum Science & Technology B

ARTICLE

avs.scitation.org/journal/jvb

Thickness dependence of infrared lattice absorption and excitonic absorption in ZnO layers on Si and SiO_2 grown by atomic layer deposition

Cite as: J. Vac. Sci. Technol. B 38, 042201 (2020); doi: 10.1116/6.0000184
Submitted: 10 March 2020 · Accepted: 4 May 2020 ·
Published Online: 26 May 2020

Nuwanjula S. Samarasingha,[1] Stefan Zollner,[1,a)] Dipayan Pal,[2] Rinki Singh,[3] and Sudeshna Chattopadhyay[2,3,4]

AFFILIATIONS

[1]Department of Physics, New Mexico State University, MSC 3D, P.O. Box 30001, Las Cruces, New Mexico 88003
[2]Discipline of Physics, Indian Institute of Technology Indore, Indore 453552, India
[3]Discipline of Biosciences and Biomedical Engineering, Indian Institute of Technology Indore, Indore 453552, India
[4]Discipline of Metallurgy Engineering and Materials Science, Indian Institute of Technology Indore, Indore 453552, India

Note: This paper is part of the Conference Collection: 8th International Conference on Spectroscopic Ellipsometry 2019, ICSE.
[a)]**Electronic mail:** zollner@nmsu.edu

ABSTRACT

Using spectroscopic ellipsometry from the midinfrared (0.03 eV) to the deep ultraviolet (6.5 eV), the authors determined the thickness dependence of the dielectric function for ZnO thin layers (5–50 nm) on Si and quartz in comparison to bulk ZnO. They observed a small blueshift of the band gap (~80 meV) in thin ZnO layers due to quantum confinement, which is consistent with a simple effective mass theory in an infinite potential well. There is a drastic reduction in the excitonic effects near the bandgap, especially for thin ZnO on Si, which not only affects the excitonic absorption peak but also lowers the high-frequency dielectric constant by up to 40%. No significant change of the phonon parameters (except an increased broadening) in thin ZnO layers was found.

I. INTRODUCTION

The dielectric function (DF) of crystalline group-IV and III/V semiconductors does not vary significantly with growth conditions, substrate, or layer thickness. For example, the DF of bulk silicon[1] is very similar to that of thick polycrystalline Si (Ref. 2) or silicon-on-insulator.[3,4] The DF of bulk GaN (Refs. 5 and 6) is nearly the same as for layers grown on sapphire,[7,8] SiC, or GaAs.[9] Differences, if any, appear primarily near the infrared-active phonon peaks or interband critical points due to strain (small shifts), disorder, or finite-size effects (shifts, broadenings), but the high-frequency dielectric constant ϵ_∞ is nearly constant.[4]

On the other hand, the DF of complex metal oxides is highly variable. Bulk[10] $SrTiO_3$ (STO), for example, has a much higher DF than thick polycrystalline STO on Si (Ref. 11) or thin polycrystalline layers of STO on Pt.[10] The high-frequency dielectric constant ϵ_∞ of epitaxial STO on Si decreases monotonically with thickness, accompanied by a Kramers–Kronig-consistent decrease in the UV absorption.[12] This was attributed to an interfacial SiO_2 layer, which becomes more important for thinner STO layers.[12] Strain-induced effects in metal oxides,[13–15] such as $BaTiO_3$ or $PbTiO_3$, are also much larger than elasto-optic effects in semiconductors.[16,17]

Without thickness and roughness measurements by x-ray reflectance (XRR, which is more accurate than electron microscopy) and atomic force microscopy (AFM), such ellipsometry results are often problematic to analyze due to parameter correlations: ellipsometry cannot determine both the optical constants and the thickness of ultrathin layers or may not be able to detect thin interfacial layers, surface roughness, or density variations.[18–20]

Similar thickness-dependent DFs were also found for several metals.[21,22] This might be due to variations in density caused by voids in the layers, island growth for ultrathin layers, or variations of the Drude parameters with the grain size.[23]

To avoid the well-known defectivity and variability of complex metal oxides,[24] such as perovskites, the present study focuses on ZnO layers. ZnO is an attractive material for applications,[25] especially for photovoltaics,[26] as a transparent conductor made of

abundant elements (alternative to indium tin oxide), and high-temperature electronics. Unique properties include a high excitonic binding energy[25] of 60 meV, good chemical and mechanical stability,[25,27] and the ability of doping[28] as an n-type conductor.[29,30]

Several studies on the variability of the optical constants of ZnO layers have already appeared.[27,31–36] Using spectroscopic ellipsometry, Logothetidis *et al.*[27] found a dependence of the optical constants of sputtered ZnO on Si on the partial pressure and thickness, but the thickness dependence was not monotonic. Nie *et al.*[31] found a quantum confinement shift of the bandgap of ZnO produced on sapphire by pulsed laser deposition. Their measured shift was 250 meV in the thinnest layers (5 nm), but this study has three flaws: the thickness was determined from x-ray diffraction (XRD) using the Scherrer formula[30] (which is not very accurate and does not determine density or roughness), the absorption coefficient was determined from transmission measurements (which might be affected by varying reflection losses due to changes in refractive index), and the absorption coefficient did not depend monotonically on thickness. Using photoluminescence of annealed ZnO layers on glass produced by DC magnetron sputtering, Mosquera *et al.*[32] found a much larger confinement shift of up to 650 meV in layers of only 10 nm. They determined thickness using a DECTAC profilometer and found the bandgap by photoluminescence, which might be related to defects rather than band edges. Li *et al.*[33] found a monotonic decrease of the DF in thinner ZnO on Si (sputtered on a 30 nm thermal SiO_2 oxide) with ellipsometry and a confinement shift of up to 140 meV in their thinnest (10 nm) layers with a grain size of 6 nm determined using the Scherrer formula and scanning electron microscopy. No independent method to determine thickness or density was used. The decrease in the DF was attributed to reductions in single-particle interband absorption and exciton-continuum absorption, while the discrete exciton absorption was affected less.[33] Their theoretical model was rather incomplete because it did not address the reasons for these changes, especially the relative weight of the discrete and continuum exciton absorption. To rule out layer density as a factor influencing the dependence of the ZnO DF on thickness, Pal *et al.*[34,35] determined the thickness, density, grain size, and roughness of ZnO on Si grown by atomic layer deposition[28] (ALD) using XRR, XRD, and AFM.[30] They found a monotonic dependence of the DF on thickness and a confinement shift of no more than 100 meV.

Given the considerable variability in the literature regarding the optical constants of ZnO thin layers, we deposited a new set of ZnO layers by ALD, with thicknesses from 5 to 69 nm. To reduce the influence of interfacial layers, we studied ZnO layers on Si as well as on SiO_2 (compare Ref. 37). We carefully determined crystallinity, surface roughness, density, and layer thickness with XRD, AFM, and XRR. To understand the physics of the variability of the DF and the influence of electronic and vibrational structure changes, we combined data over a broad spectral range, from the midinfrared (0.03 eV) to the deep ultraviolet (6.6 eV).

We find significant variations of the optical constants of ZnO as a function of thickness. The role of the substrate (Si or quartz) is also very important. The excitonic direct-gap peak is strongly broadened and weakened in thinner layers. The infrared-active E_1 phonons are also broadened due to finite-size effects. The blueshift of the bandgap due to quantum confinement is smaller than reported before but in excellent agreement with a simple theoretical model. Our most striking result is a 40% reduction in the high-frequency dielectric constant in thin layers on Si, which we explain with a shift of the oscillator strength to higher photon energies due to the weakening of the excitonic electron-hole attraction.

II. EXPERIMENTAL METHODS AND RESULTS

Wurtzite-type ZnO films with preferred c axis orientation were grown at 200 °C on single-side polished Si (001) and SiO_2 (fused amorphous quartz) substrates using ALD (BENEQ TFS 200 reactor, Espoo, Finland) with diethylzinc and water as precursors and nitrogen as a carrier and purge gas, as described elsewhere.[34,35] Large-area uniform layers for shallow-angle ellipsometry and XRR measurements were produced by growth on 20×20 mm^2 substrates. By varying the number of ALD growth cycles from 30 to 410, layer thicknesses between 5 and 70 nm could be achieved, as measured using XRR. The growth rate of ZnO was ~1.7 Å per cycle. Table SI gives an overview of the samples with XRR characterization results.[75] Layers on Si had an interfacial oxide with a thickness of ~1 nm. The surface roughness was also ~1 nm, much less than for sputtered ZnO layers,[27,32,38,39] and agreed well between AFM and XRR (see Fig. S1).[75] Most layers had an electron density just below that of bulk ZnO, except for the thinnest layers on SiO_2, for which it was ~10% lower. See supplemental material[75] for more information regarding the characterization of the layers with AFM, XRD, and XRR.

The ellipsometric angles[18,19] ψ and Δ of the as-received layers (without cleaning) were acquired from 0.03 to 6.5 eV at three angles of incidence (60°, 65°, and 70°) on two different instruments. A J. A. Woollam FTIR-VASE instrument was used to measure in the mid- and near-infrared spectral regions from 0.03 to 0.6 eV. A J. A. Woollam VASE instrument provided data from 0.5 to 6.5 eV (near-infrared to deep ultraviolet). The overlap in the region between 0.5 and 0.6 eV (where data were taken on both instruments) is good but not perfect. All measurements were performed in air at 300 K. Typical spectra for thin and thick ZnO on Si and SiO_2 are shown in Figs. 1–4. Strong anisotropy effects[40] were seen in thick ZnO layers on quartz.

III. DIELECTRIC FUNCTION MODELS

We extract the dielectric functions for the ZnO layers on Si (Ref. 1) by fitting the ellipsometric angles versus angular frequency ω with an isotropic model for ZnO (Ref. 41),

$$\epsilon(\omega) = \frac{\omega_{LO}^2 - \omega^2 - i\gamma_{LO}\omega}{\omega_{TO}^2 - \omega^2 - i\gamma_{TO}\omega}\left[1 + \sum_i g_i(\omega)\right]\prod_i [1 + G_i(\omega)], \quad (1)$$

similar to the model (S3) for bulk ZnO described in the supplemental material.[75] This model allows us to describe the entire dielectric function from the midinfrared to the deep ultraviolet with a single equation, while retaining the option of different broadening parameters γ for the transverse optical (TO) and longitudinal optical (LO) phonons. The first factor[42] contains the infrared lattice response, while the second factor describes the electronic

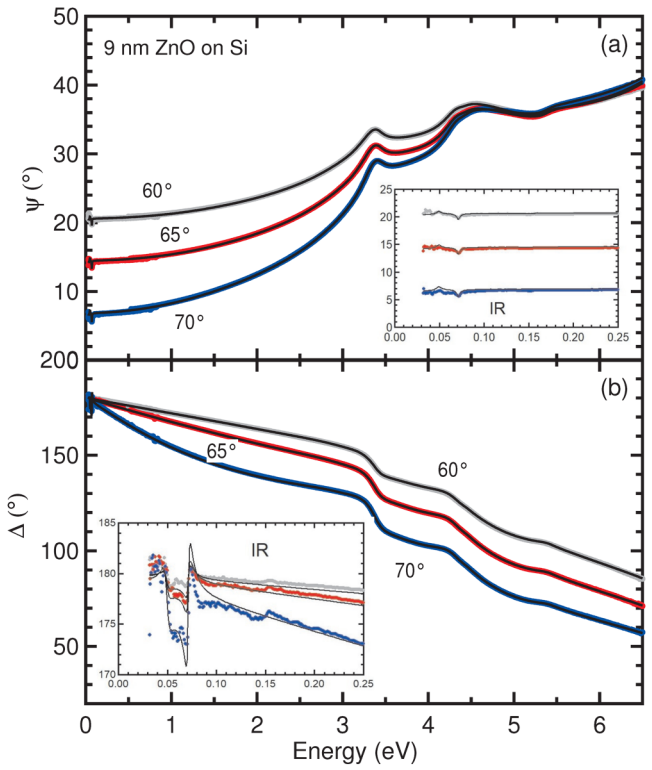

FIG. 1. Ellipsometric angles ψ and Δ for 9 nm ZnO on Si. Symbols: experimental data; solid: best fit with an isotropic model based on Eq. (1). The inset shows a magnified view of the infrared spectral region from 0 to 0.25 eV.

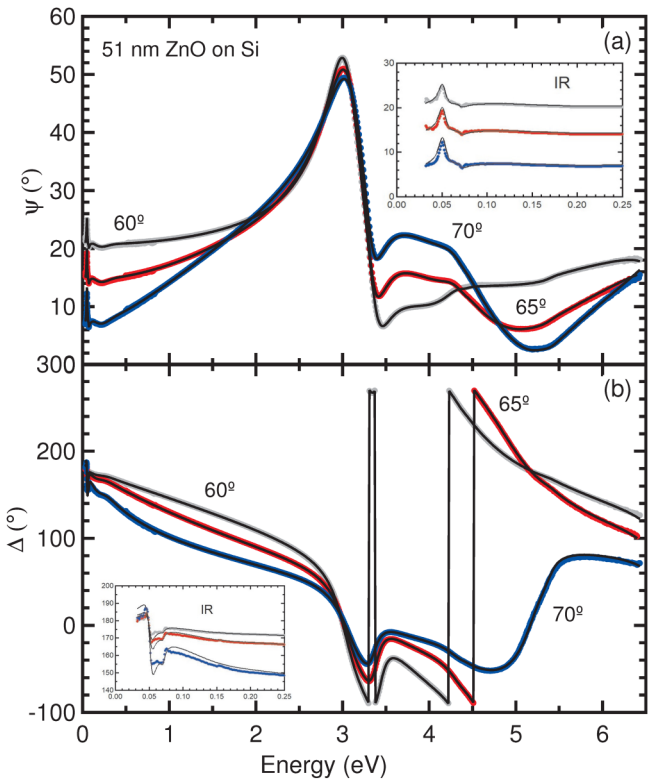

FIG. 2. As Fig. 1, but for 51 nm ZnO on Si.

response with oscillator functions $g_i(\omega)$, such as Tauc–Lorentz or Herzinger–Johs parametric oscillators.[1,19] The third factor, which is not needed for bulk ZnO, contains complex Gaussian functions $G_i(\omega)$ with an imaginary part

$$\mathrm{Im}[G(\omega)] = Ae^{-\left(\frac{\omega-E}{\sigma}\right)^2} - Ae^{-\left(\frac{\omega+E}{\sigma}\right)^2} \quad (2)$$

and a Kramers–Kronig-consistent real part. It describes an anomalous broad infrared absorption, perhaps related to defects, such as oxygen vacancies.[43] These Gaussians are required to describe the optical constants for some of the thicker ZnO layers, especially on quartz. The Gaussian oscillator has three parameters, a dimensionless amplitude A, a resonance energy E, and a FWHM broadening $\Gamma = 2\sigma\sqrt{\ln 2}$. At the most two Gaussians were needed to achieve a good fit to the ellipsometric angles. Gaussian parameters are listed in Tables I and II along with the TO and LO parameters.

For ZnO on Si, our model consists of the following layers: ambient, roughness, ZnO layer, interfacial SiO_2, and Si substrate. The ZnO layer thickness on Si was treated as a parameter shown in Table SI.[75] SE and XRR find very similar results for the ZnO layer thickness. The interfacial SiO_2 layer thickness was fixed at 1 nm. The roughness layer thickness was obtained from the XRR results in Table SI.[75] The entire model for ZnO on Si has 25–31 free parameters, including the ZnO thickness, four TO/LO energies and broadenings, three parameters for each Gaussian, four for the Tauc–Lorentz oscillator, seven for each simplified parametric oscillator, and two for the UV pole. We started by fitting the TO/LO and Gaussian parameters to the ellipsometric angles in the infrared spectral region, taking the UV parameters from the bulk as a starting point. Then, we also adjusted the UV parameters by fitting the entire dataset. To avoid instabilities in the IR to UV fit, we had to fix some infrared parameters to the values obtained by fitting the infrared dataset. These parameters are marked (f) in Tables I and II. For the fit of the thinnest ZnO layers on Si, we had to enforce the condition[42] $\Gamma_{LO} \geq \Gamma_{TO}$.

To determine the dielectric functions for ZnO on SiO_2 (quartz), we first obtained the dielectric function of quartz from measurements of a bare substrate, see supplemental material,[75] especially Fig. S7.[75] We proceeded in a similar fashion to fit the ellipsometric angles for ZnO on quartz as on Si. However, the thickest ZnO layers on SiO_2 required a partially anisotropic model (with different phonon energies and broadenings in the ordinary and extraordinary direction and a constant birefringence offset $\epsilon_{\infty e} - \epsilon_{\infty o} = 0.08$), see Sec. S4. This model contained the following layers: ambient, roughness, ZnO layer, and quartz substrate. We did not include an interfacial layer in this model because we do not know how the

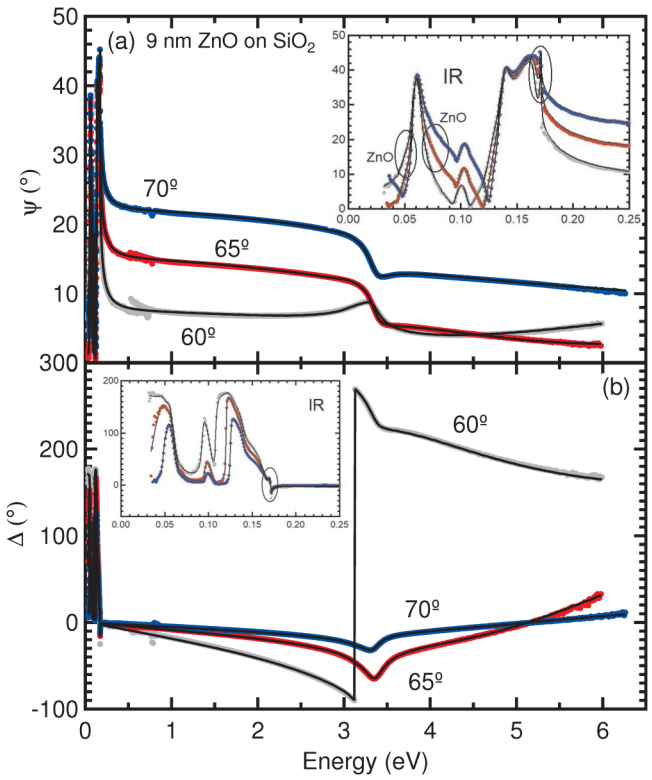

FIG. 3. As Fig. 1, but for 9 nm ZnO on SiO_2. ZnO vibrational features affect the spectra mostly within the ovals.

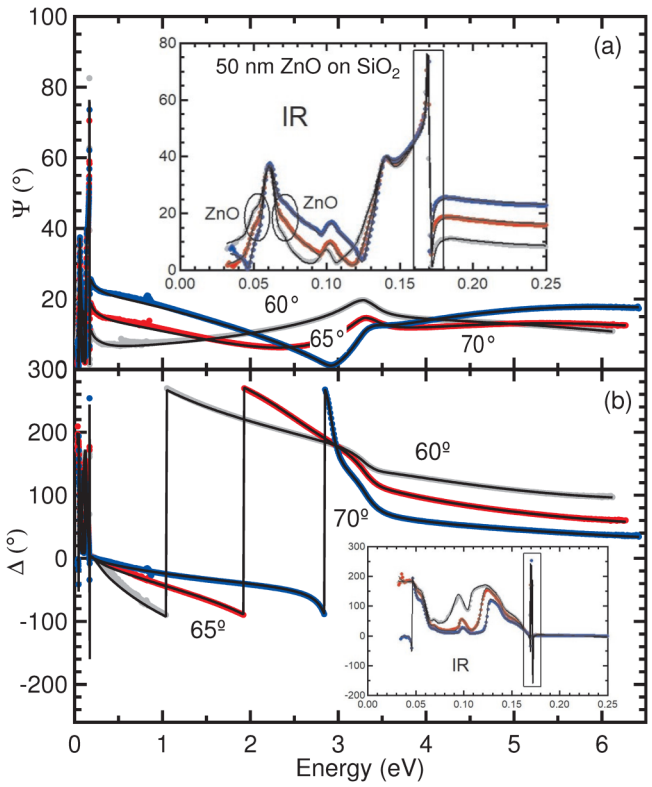

FIG. 4. As Fig. 3, but for 50 nm ZnO on SiO_2 with a partially anisotropic model for ZnO. Effects of ZnO anisotropy appear within the rectangular boxes.

substrate clean and the ALD growth affected the quartz substrate surface. Our data did not require a fully anisotropic treatment of the optical constants.[44]

After these oscillator fits were completed and the ZnO layer thickness determined, we also performed independent wavelength-by-wavelength (or point-by-point) fits, where the thickness was fixed and the real and imaginary parts of the dielectric function treated as free parameters at each wavelength. Both methods resulted in very similar dielectric functions (see Figs. S8 and S9),[75] but the point-by-point dielectric function is usually noisier than the oscillator fit.

IV. ELLIPSOMETRY ANALYSIS

The dielectric functions for ZnO layers on Si and SiO_2 with various thicknesses between 5 and 51 nm are shown in Figs. 5 and 6. Data for bulk ZnO, determined as described in the supplementary material[75] and in good agreement with prior ellipsometry measurements[46,47] and theory,[48] are also shown for comparison. Both ϵ_1 and ϵ_2 show significant variations with thickness over the complete spectral range, regardless of the substrate.

For ZnO on Si, the absorption above the bandgap (say, at 4 eV) increases monotonically with the layer thickness. The exciton-phonon complexes[49–52] are not visible in the ZnO layers, only in the bulk.

TABLE I. Longitudinal (LO) and transverse optical (TO) phonon energies E and broadenings Γ (errors in parentheses) of ZnO films on Si compared to the bulk for the ordinary (o) and extraordinary (eo) beams. Some films required additional Gaussian (G) oscillators with dimensionless amplitude A, energy E, and broadening Γ (both in cm^{-1}). Parameters marked (f) were adjusted to the infrared portion of the data and then fixed during the fit over the whole range.

		E_{TO} (cm^{-1})	Γ_{TO} (cm^{-1})	E_{LO} (cm^{-1})	Γ_{LO} (cm^{-1})
Bulk	o	408.75(6)	9.7(1)	589.67(5)	9.76(8)
	eo	378.9(5)	8(f)	574.3(1)	8.13(4)
Bulk[a]	o	408.2(3)		592.1(2)	
	eo	379(2)		577.1(4)	
51 nm		410(f)	61(f)	573(f)	75(f)
	G	A=3.8(f)	E=82(f)	Γ=1560(f)	
	G	A=2.4(f)	E=210(f)	Γ=2475(f)	
37 nm		402(f)	37(3)	577(f)	75(f)
19 nm		401(4)	41(f)	578(4)	50(5)
9 nm		399(f)	55(f)	575(5)	Same as Γ_{TO}
5 nm		376(f)	55(f)	562(5)	Same as Γ_{TO}

[a]Reference 45.

TABLE II. As Table I, but for ZnO films on SiO_2. The fit is not sensitive to the values shown in italics, which were chosen arbitrarily.

		E_{TO} (cm^{-1})	Γ_{TO} (cm^{-1})	E_{LO} (cm^{-1})	Γ_{LO} (cm^{-1})
50 nm	o	403(f)	45(f)	591(f)	288 (f)
	eo	380(f)	*45*	580(f)	58 (f)
	G	*A*=1.6(f)	*E*=329(f)	Γ=1607(f)	
	G	*A*=0.9(f)	*E*=219(f)	Γ=231(f)	
38 nm	o	403(f)	74(f)	577(f)	180(f)
	eo	380(f)	*74*	581(f)	52(f)
	G	*A*=0.8(f)	*E*=577(f)	Γ=1376(f)	
19 nm	o	402(f)	70(f)	584(f)	118(f)
	eo	380(f)	70(f)	587(5)	41(f)
	G	*A*=0.47(f)	*E*=577(f)	Γ=1406(f)	
9 nm		399(f)	*83*	589(f)	95(f)
5 nm[a]		*376*	*90*	*558*	*90*

[a]Assuming identical parameters as for ZnO on Si.

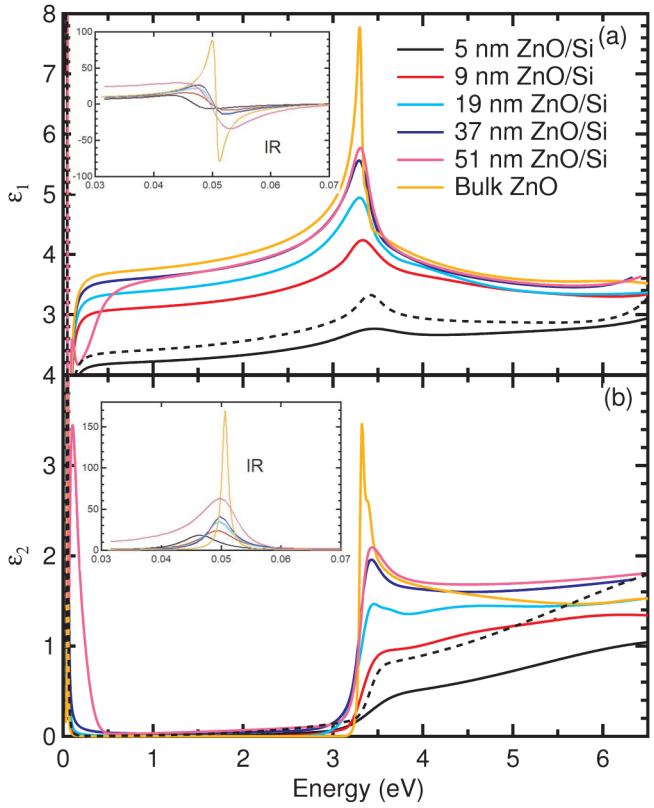

FIG. 5. Real and imaginary parts of the complex dielectric function for ZnO films on Si vs photon energy. The inset shows a magnified view of the infrared spectral region from 30 to 70 meV. The dotted lines are explained in Sec. S11 (Ref. 75).

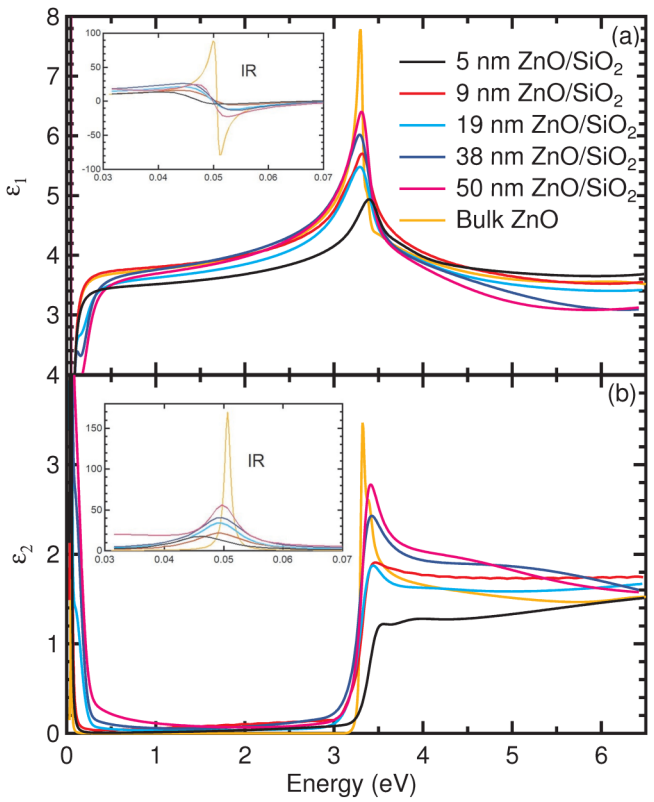

FIG. 6. As Fig. 5, but for ZnO on SiO_2 (quartz).

The excitonic enhancement of the absorption is much weaker in the ZnO layers (especially the thinner ones) than in bulk ZnO. The excitonic peak is broadened and completely disappears for the 5 and 9 nm thick ZnO layers on Si. The Tauc gap E_g determined from a Tauc plot (αE vs $\sqrt{E}$, see Sec. S7)[75] increases for thinner layers and can be described with a confinement model[53]

$$E_g(t) = E_{g,\infty} + \frac{F}{t^2} - \Delta E, \tag{3}$$

see Fig. 7(a), where $E_{g,\infty} = 3.29$ eV is the bulk ZnO Tauc gap, t is the layer thickness, F is the confinement factor (equal to $\hbar^2\pi^2/2\mu_{eh}$ for infinitely high barriers, where μ_{eh} is the electron-hole reduced effective mass), and ΔE is a thickness-independent difference between the bulk and layer Tauc gap (for example, due to defects, doping, etc.). The bulk Tauc gap (determined by linear extrapolation of a Tauc plot as shown in Sec. S7)[75] is ~80 meV lower than the bulk bandgap of ZnO, usually given as 3.37 eV, see Ref. 47. The blueshift between our thinnest (5 nm) and thickest (51 nm) layers is no more than 80 meV, lower than what has been reported in the literature for other ZnO layers.[31–33] For the thickest ZnO layer (51 nm) on Si, there is a strong Gaussian absorption of unknown origin, with parameters given in Table I. ϵ_1 drops toward the infrared spectral region due to

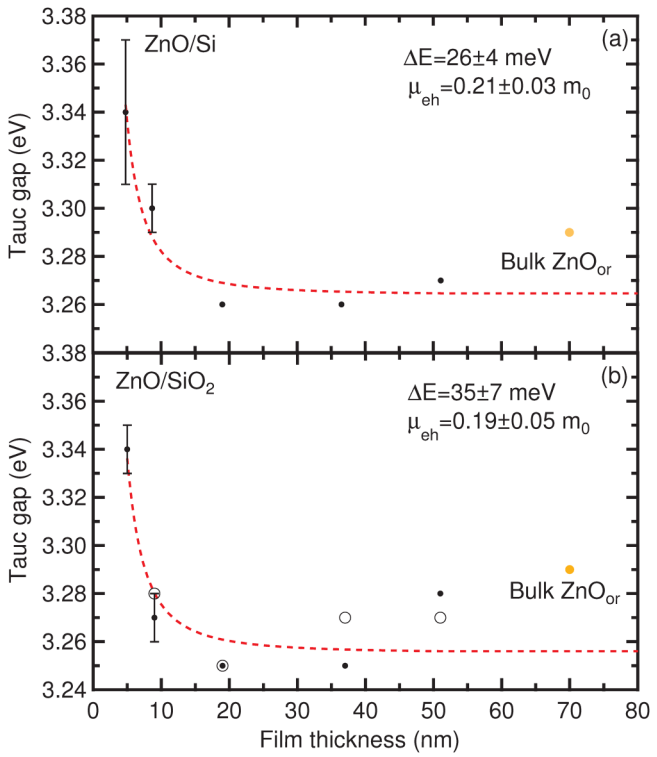

FIG. 7. Tauc bandgap of ZnO on Si (a) and SiO_2 (b) as a function of layer thickness from ellipsometry (•) and transmission measurements (○). The dotted line shows the best fit with Eq. (3).

the dispersion related to infrared lattice absorption. For the thickest (51 nm) layer, ϵ_1 drops earlier (near 1 eV) and reaches a minimum near 0.2 eV due to the unknown Gaussian absorption.

The dependence of ϵ_1 on thickness for ZnO on Si is Kramers–Kronig consistent with the dependence of ϵ_2. The excitonic enhancement of ϵ_1 near the bandgap becomes weaker and is broadened in thinner films. In addition, there is a drastic reduction (by 40%) in ϵ_∞, determined from the second factor in Eq. (1) by setting $\omega = 0$, for thinner films [see Fig. 8(b)]. The differences of ϵ_1 between thinner and thicker films diminish toward higher energies. Unfortunately, we are not able to measure beyond 6.5 eV.

The thickness dependence of the optical constants for ZnO on quartz is qualitatively similar to the behavior on Si but weaker. The excitonic peak at the bandgap is not broadened as strongly in ZnO on SiO_2. This makes it easier to see the blueshift due to confinement [see Fig. 7(b)]. Also, the absorption does not drop off as rapidly as the thickness decreases. The unknown infrared Gaussian absorption is present in several layers on SiO_2. The high-frequency dielectric constant ϵ_∞ is nearly independent of thickness [see Fig. 8(b)].

The phonon parameters used in these fits are given in Tables I and II. The values of the TO phonon energies versus layer thickness are shown in Fig. 9 in comparison to the bulk.[45] From the TO and LO angular frequencies of the E_1 phonon, we can calculate the

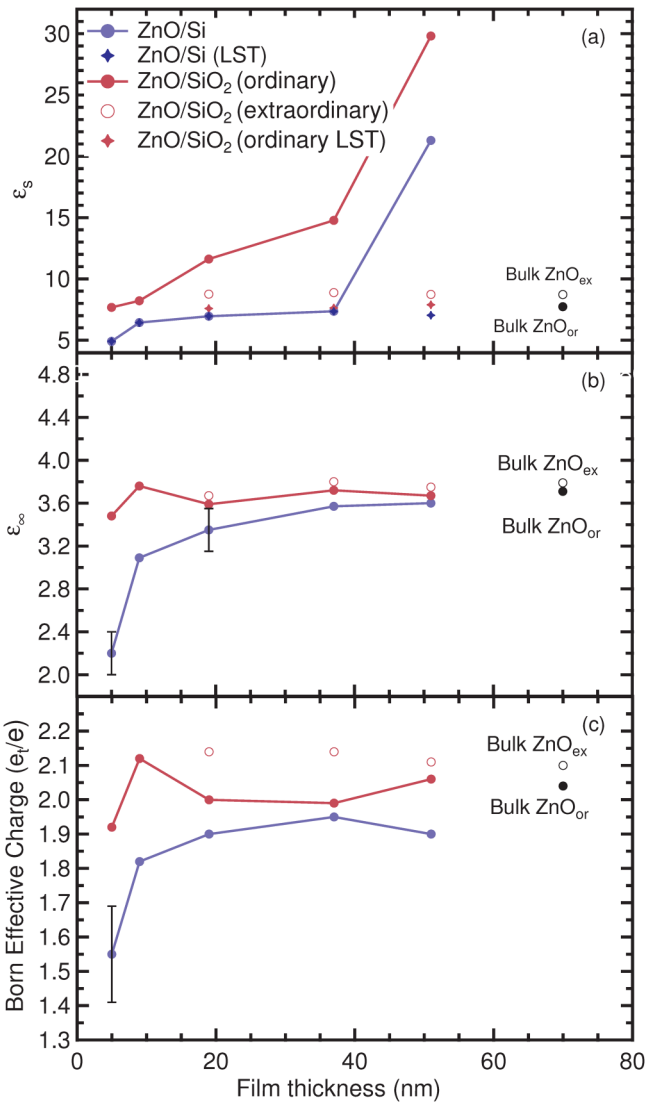

FIG. 8. (a) Static dielectric constant ϵ_s calculated from Eq. (1) by setting $\omega = 0$ (•, ○) and calculated from the TO and LO energies using the Lyddane–Sachs–Teller (LST) relation (9) (✦). (b) Thickness dependence of the high-frequency dielectric constant ϵ_∞, determined from the second factor in Eq. (1) by setting $\omega = 0$. (c) Born effective charge of E_1 (•) and A_1 (○) optical phonon calculated from Eq. (4) for ZnO on Si (blue) and on SiO_2 (red). The lines are drawn to guide the eye.

Born effective charge[54]

$$(e_t^*)^2 = V\mu\epsilon_0\epsilon_\infty(\omega_{LO}^2 - \omega_{TO}^2), \tag{4}$$

see Fig. 8(c), where ϵ_0 is the vacuum permittivity and ϵ_∞ is the high-frequency dielectric constant. μ is the reduced mass of the Zn and O atoms. V is the volume per ZnO formula unit.

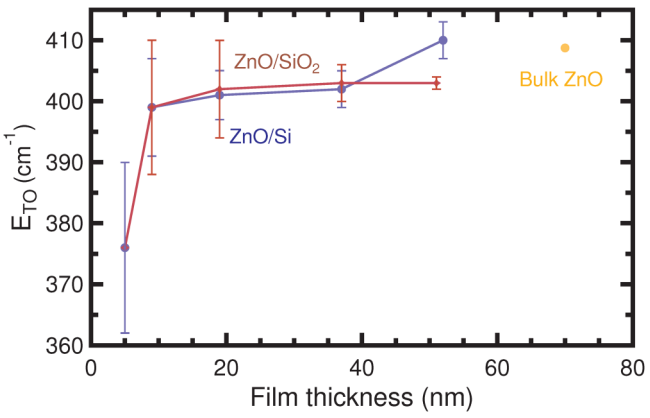

FIG. 9. Transverse optical (E_1 TO) phonon energies vs layer thickness for ZnO on Si and SiO_2 in comparison with bulk ZnO.

V. DISCUSSION

A. Quantum confinement

ZnO layers on Si and quartz show a confinement shift of ~80 meV for 5 nm thickness (for both types of substrates), see Fig. 7. This result is reasonable, similar to what has been found for InGaAs quantum wells with InP barriers.[55] Fitting the bandgap versus thickness using Eq. (3) yields two parameters $\Delta E \approx 30$ meV and $\mu_{eh} \approx 0.2$, as shown in Fig. 7. These parameters are nearly the same for both substrates. The value of μ_{eh} from our confinement fit is very similar to the reduced excitonic effective mass determined from fits to optical spectra (photoreflectance and photoluminescence).[56] The corresponding electron and hole effective masses are 0.29 and 0.66, respectively.[56]

B. High-frequency dielectric constant

The second significant result is that the high-frequency dielectric constant ϵ_∞ is nearly independent of the layer thickness for ZnO on SiO_2 but drops by 40% in the thinnest ZnO layers on Si (see Fig. 8). How do we explain this? ϵ_∞ is given by[57,58]

$$\epsilon_\infty = 1 + \left(\frac{\omega_{\mathrm{pl}}}{\omega_{\mathrm{Penn}}}\right)^2 S_0, \tag{5}$$

where

$$\omega_{\mathrm{pl}}^2 = \frac{\rho e^2}{\epsilon_0 m_0} \tag{6}$$

is the unscreened plasma frequency, ω_{Penn} is the Penn gap, and S_0 is a constant typically assumed to be unity.[57] The electron density ρ is the total number of electrons per unit cell divided by the unit cell volume. This number only depends on the elements in our compound (Zn and O, 8 electrons per formula unit) and the cell volume. Since the XRR density varies by <10% (see Sec. S3)[75] and varies more for ZnO on SiO_2 than on Si, variations in density (or plasma frequency) cannot explain the observed changes in ϵ_∞.

On the other hand, the Penn gap ω_{Penn} is the energy separation between the bonding and antibonding sp^3 hybrids, averaged in k-space over all bands. This Penn gap becomes smaller if the excitonic electron-hole interactions are turned on, which shifts the oscillator strength to lower energies.[59,60] Variations of the Penn gap (and thus ϵ_∞) can, therefore, be explained with variations of the excitonic interactions.

The dependence of S_0 on excitonic effects was recently discussed by Cirilo-Lombardo.[61] In the absence of excitonic effects, $S_0 = 1$ (Penn's[57] result). If excitonic effects are considered, then $S_0 = \frac{2}{3}$. Therefore, as the excitonic peak becomes stronger, ϵ_∞ should decrease; as the excitonic peak becomes weaker, ϵ_∞ should increase (if the Penn gap remains constant). This is the opposite of what we observe and, therefore, the impact of the excitonic interaction on S_0 does not explain our observations.

We pointed out previously[35] that the band alignments at ZnO interfaces with Si and SiO_2 are very different.[62,63] ZnO/SiO_2 is a type-I interface where both electron and hole are confined in the ZnO well by the SiO_2 barrier. Therefore, strong excitonic effects are expected in ZnO/SiO_2 quantum wells. On the other hand, ZnO/Si is a type-II (staggered) interface. While electrons are confined in the ZnO layer, holes will diffuse into the Si substrate, especially if the ZnO layer is thin (see Fig. 9 in Ref. 35). This will break apart the exciton and thus lead to an increase of the Penn gap, which reduces ϵ_∞, as we observe.

We can also invoke the optical conductivity sum rule[64]

$$\omega_{\mathrm{pl}}^2 = \frac{2}{\pi}\int_0^\infty \epsilon_2(\omega)\omega\, d\omega. \tag{7}$$

Since the electron density ρ (and, therefore, ω_{pl}) is nearly constant, reducing $\epsilon_2(\omega)$ near the bandgap (as excitonic effects are weakened) requires a shift of the oscillator strength to higher energies (outside of our spectral range) to keep the integral nearly constant. To clarify this point, it would be useful to measure optical constants beyond 6.5 eV, perhaps in a nitrogen-purged ellipsometer,[10] at a synchrotron,[60] or with a high-harmonic femtosecond laser source.[65] The experimental problem with such measurements is that the importance of surface roughness increases as the photon energy gets larger.

The other sum rule[64]

$$\epsilon_\infty = 1 + \frac{2}{\pi}\int_0^\infty \frac{\epsilon_2(\omega)}{\omega}\, d\omega \tag{8}$$

directly relates the high-frequency dielectric constant to an integral containing the imaginary part of the dielectric function ϵ_2. As excitonic effects are reduced in ZnO layers on Si, the oscillator strength is shifted to higher photon energies,[59,60] which clearly reduces ϵ_∞ from Eq. (8) because the denominator is larger for higher photon energies.

C. Decreased absorption

It can be seen clearly from Figs. 5 and 6 that the magnitude of ϵ_2 decreases in thinner films. It decreases more in ZnO on Si due to the weakening of excitonic effects (as discussed above in Subsection V B) but to a lesser extent also in ZnO on SiO_2. The decreased absorption is described by the imaginary part ϵ_2 of the dielectric function, which is related to its real part ϵ_1 through the Kramers–Kronig transform.[19,64] It can be seen in Fig. 5 that ϵ_2 for bulk ZnO decreases toward higher photon energies, while ϵ_2 for the thinnest layers increases at higher energies. This may be a reflection of the shift of the oscillator strength toward higher energies as the excitonic effects are decreased.

Excitonic contributions to the absorption and dispersion of semiconductors are described by the Elliot–Tanguy theory.[66,67] The parameters of this theory are the bulk bandgap, its broadening, the strength of the bandgap absorption (amplitude; related to the effective masses of electrons and holes, the transition matrix element, and fundamental constants), the exciton binding energy, and the excitonic screening parameter. This Tanguy oscillator is included in commercial software (WVASE32) and can be used to fit the ellipsometric angles. However, in the case of ZnO, one also needs to consider the exciton-phonon complexes. This introduces two additional parameters, the phonon energy and the exciton-phonon coupling constant.[51,52] Unfortunately, fitting the ellipsometric angles while including the excitonic effects and exciton-phonon complexes is not currently possible in commercial software. There is an explicit theory for the imaginary part,[51,52] but not for the real part of the dielectric function. Therefore, a fit to our ellipsometric angles including excitonic effects and exciton-phonon complexes (to determine exciton and exciton-phonon coupling parameters) is beyond the scope of our current work. We note that it is possible to determine the imaginary part of ϵ from a point-by-point fit as shown in Figs. S8 and S9 (Ref. 75), and then fit this result with the Elliot theory for ϵ_2, including exciton-phonon complexes.[51,52] However, this approach does not properly include the experimental errors of the ellipsometric angles as a function of photon energy. It may also lead to results that are not Kramers–Kronig consistent.

Therefore, we confine our discussion to the experimental finding that the excitonic absorption peaks near the ZnO bandgap are significantly reduced in amplitude as well as broadened in ZnO layers on both Si and SiO_2. We qualitatively conclude that excitonic effects are weakened in thin layers, especially on Si, but defer a quantitative treatment of these effects to future work.

D. Phonon energies and born effective charge

From our infrared ellipsometry data, it is difficult to determine if the TO and LO energies of the E_1 phonon depend on layer thickness (see Fig. 9). For the thinnest ZnO layers on Si, the TO absorption peaks are very weak and broad (see Figs. 5 and 6), which leads to large errors of the TO energies that do not allow a clear statement about phonon softening at small thicknesses. For ZnO on SiO_2, even for our thickest layers, the ZnO vibrational features are just minor corrections to the strong infrared response of quartz (see Fig. 4).

In the bulk,[45] the E_1 TO and LO energies are $\sim$408 cm^{-1} (50.6 meV) and 590 cm^{-1} (73.2 meV), respectively, compare Table I. Theory states[68–70] that a reduction in the particle size (in ZnO nanoparticles) leads to a broadening in k-space, which is on the order of 20% of the Brillouin zone radius for a particle with a 5 nm diameter. This k-space uncertainty leads to a (possibly asymmetric) broadening and a redshift or blueshift (depending on the phonon dispersion curvature) of optical phonon peaks, as observed in our experiments on thin ZnO layers. The shifts and broadenings in thin layers are not very large, however, because the dispersion of the E_1 phonon near the Γ-point is rather flat.[71] A redshift and broadening of the E_1 LO phonon was indeed observed in ZnO nanoparticles with Raman spectroscopy.[72] However, it was pointed out that laser heating in resonant Raman spectroscopy with a UV laser will also cause a redshift,[73] putting the results of Ref. 72 in question.

In an ellipsometry measurement of a c axis textured layer, the electric field vector interacts with E_1 phonons, which have atomic displacements in the plane of the layer. This in-plane dimension is not confined by the thickness of a thin layer, only by the lateral extension of grains. However, the wave vector of the excited phonon is equal to the wave vector of the photon (perpendicular to the layer) and therefore confined by the layer thickness. In other words, while the motion of the atoms is not confined by the thin layer, the uncertainty of the phonon wave vector is affected by the finite layer thickness. Therefore, the shift of the E_1 phonon energy in a thin layer should be similar to a nanoparticle, which is confined in all three directions.

The E_1 LO phonon is not observable in bulk ZnO crystals with infrared transmission or ellipsometry experiments because this phonon does not couple with infrared light. However, in thin layers, the so-called Berreman effect[74] causes a structure in the ellipsometric angles at the LO energy, which is clearly observable even for a 9 nm thick ZnO layer on Si, compare Fig. 1. A softening of the E_1 LO phonon energy by 20–30 cm^{-1} is possible (similar to the softening of the E_1 TO phonon shown in Fig. 9), but the errors are rather large.

We, therefore, prefer not to make a definitive statement about the thickness dependence of the E_1 phonon energies and do not discuss this phenomenon quantitatively. Assuming a Gaussian line shape for TO phonon absorption may not be the optimal approach for ultrathin layers, but adding additional parameters to describe asymmetry is not supported by the ellipsometric angles and the low signal to noise ratio in our spectra.

From the TO and LO phonon energies, we can also calculate the Born effective charge [see Eq. (4) and Fig. 8(c)]. The Born effective charge follows the same trends as the high-frequency dielectric constant [see Fig. 8(b)]: It is nearly independent of thickness for ZnO on SiO_2 but decreases significantly (by $\sim$20%) for ZnO on Si. The difference of the squares of the LO and TO phonon energies changes much less (see Table I).

E. Static dielectric constant

The static dielectric constant ϵ_s can be calculated in two different ways: First, we can set $\omega = 0$ in Eq. (1), which directly yields ϵ_s in our WVASE ellipsometry software. These results are shown by circles in Fig. 8(a). We find that thicker layers have much larger static dielectric constants than the bulk because of the strong infrared Gaussian absorption of unknown origin, which also contributes to ϵ_s by the Kramers–Kronig transform.

The static dielectric constants

$$\epsilon_s = \epsilon_\infty \frac{\omega_{LO}^2}{\omega_{TO}^2} \tag{9}$$

calculated from the Lyddane–Sachs–Teller relations[64] shown by crosses in Fig. 8(a) are much closer to the bulk values, which gives us confidence in our results for ϵ_∞ and the optical phonon energies. We conclude that the static dielectric constant is influenced by defect absorption much more than by changes in the E_1 phonon energies. To a lesser extent, ϵ_s is also influenced by the thickness dependence of ϵ_∞, but the ratio of the E_1 LO and TO phonon energies is nearly constant.

VI. SUMMARY

We used broad-band spectroscopic ellipsometry from 0.03 to 6.6 eV to investigate the origin of the variability of the optical constants of ZnO thin films on two different substrates (Si and quartz). The blueshift of the bandgap with decreasing layer thickness is small. It follows a simple inverse-square law due to confinement in a quantum well with infinitely high barriers. On the other hand, there is a very significant decrease of excitonic effects in thin layers, especially for ZnO on Si, leading to a reduction in the excitonic absorption, a broadening of the exciton peak, and a corresponding decrease of the high-frequency dielectric constant. Since excitonic effects shift the oscillator strength from higher to lower photon energies, our results are fully consistent with the sum rules for optical constants. We speculate that the exciton is stabilized by type-I ZnO/SiO_2 heterojunctions but breaks apart near type-II ZnO/Si interfaces. Surface electric fields in thin ZnO layers may also play a role.

ACKNOWLEDGMENTS

This work was supported by the National Science Foundation (NSF, No. DMR-1505172). The authors are grateful to Adam Dubroka and Daniel Franta at Masaryk University (Brno, Czech Republic) for reminding us of the importance of sum rules and to Oliver Herrfurth (Universität Leipzig, Germany) for sharing his insights on exciton-phonon complexes.

REFERENCES

[1]C. M. Herzinger, B. Johs, W. A. McGahan, J. A. Woollam, and W. Paulson, J. Appl. Phys. **83**, 3323 (1998).
[2]S. Zollner *et al.*, in *Amorphous and Microcrystalline Silicon Technology—1998*, edited by R. Schropp, H. M. Branz, M. Hack, I. Shimizu, and S. Wagner (Materials Research Society, Pittsburgh, 1998), p. 957.
[3]S. Zollner *et al.*, Appl. Phys. Lett. **76**, 46 (2000).
[4]J. Price and A. C. Diebold, J. Vac. Sci. Technol. B **24**, 2156 (2006).
[5]V. Darakchieva, B. Monemar, A. Usui, M. Saenger, and M. Schubert, J. Cryst. Growth **310**, 959 (2008).
[6]S. Shokhovets, M. Himmerlich, L. Kirste, J. H. Leach, and S. Krischok, Appl. Phys. Lett. **107**, 092104 (2015).
[7]G. Yu, G. Wang, H. Ishikawa, M. Umeno, T. Soga, T. Egawa, J. Watanabe, and T. Jimbo, Appl. Phys. Lett. **70**, 3209 (1997).
[8]A. Kasic, M. Schubert, S. Einfeldt, D. Hommel, and T. E. Tiwald, Phys. Rev. B **62**, 7365 (2000).
[9]R. Goldhahn, Acta Phys. Polon. **104**, 123 (2003).
[10]S. Zollner *et al.*, J. Vac. Sci. Technol. B **18**, 2242 (2000).
[11]C. V. Weiss, J. Zhang, M. Spies, L. S. Abdallah, S. Zollner, M. W. Cole, and S. P. Alpay, J. Appl. Phys. **111**, 054108 (2012).
[12]S. Zollner, A. A. Demkov, R. Liu, J. A. Curless, Z. Yu, J. Ramdani, and R. Droopad, in *Recent Developments in Oxide and Metal Epitaxy—Theory and Experiment*, edited by M. Yeadon, S. Chiang, R. F. C. Farrow, J. W. Evans, and O. Aucielo (Materials Research Society, Pittsburgh, 2000), p. 167.
[13]E. Chernova, O. Pacherova, D. Chvostova, A. Dejneka, T. Kocourek, M. Jelinek, and M. Tyunina, Appl. Phys. Lett. **106**, 192903 (2015).
[14]A. Dejneka, D. Chvostova, O. Pacherova, T. Kocourek, M. Jelinek, and M. Tyunina, Appl. Phys. Lett. **112**, 031111 (2018).
[15]A. Dejneka and M. Tyunina, Adv. Appl. Ceram. **117**, 62 (2018).
[16]S. Zollner, C. M. Herzinger, J. A. Woollam, S. S. Iyer, A. P. Powell, and K. Eberl, Solid State Commun. **96**, 305 (1995).
[17]S. Zollner, J. P. Liu, P. Zaumseil, H. J. Osten, and A. A. Demkov, Semicond. Sci. Technol. **22**, S13 (2007).
[18]H. G. Tompkins and J. N. Hilifiker, *Spectroscopic Ellipsometry: Practical Application to Thin-Film Characterization* (Momentum, New York, 2016).
[19]H. Fujiwara, *Spectroscopic Ellipsometry* (Wiley, Chichester, 2007).
[20]J. N. Hilfiker, J. Sun, and N. Hong, in *Spectroscopic Ellipsometry for Photovoltaics*, edited by H. Fujiwara and R. W. Collins (Springer, Cham, 2018), Vol. 1.
[21]G. K. Pribil, B. Johs, and N. J. Ianno, Thin Solid Films **455–456**, 443 (2004).
[22]N. Leick, J. W. Weber, A. J. M. Mackus, M. J. Weber, M. C. M. van de Sanden, and W. M. M. Kessels, J. Phys. D Appl. Phys. **49**, 115504 (2016); *ibid.* **49**, 269601 (2016).
[23]V. K. Kamineni, M. Raymond, E. J. Bersch, B. B. Doris, and A. C. Diebold, J. Appl. Phys. **107**, 093525 (2010).
[24]V. Longo, N. Leick, F. Roozeboom, and W. M. M. Kessels, ECS J. Solid State Sci. Technol. **2**, N15 (2013).
[25]Ü. Özgür, Ya. I. Alivov, C. Liu, A. Teke, M. A. Reshchikov, S. Doğan, V. Avrutin, S.-J. Cho, and H. Morkoç, J. Appl. Phys. **98**, 041301 (2005).
[26]B. Hussain, A. Aslam, T. M. Khan, M. Creighton, and B. Zohuri, Electronics **8**, 238 (2019).
[27]S. Logothetidis, A. Laskarakis, S. Kassavetis, S. Lousinian, C. Gravalidis, and G. Kiriakidis, Thin Solid Films **516**, 1345 (2008).
[28]Z. Gao and P. Banerjee, J. Vac. Sci. Technol. A **37**, 050802 (2019).
[29]H. Fujiwara and M. Kondo, Phys. Rev. B **71**, 075109 (2005).
[30]E. Pereira da Silva, M. Chaves, S. F. Durrant, P. N. Lisboa-Filho, and J. R. R. Bortoleto, Mater. Res. **17**, 1384 (2014).
[31]J. C. Nie, J. Y. Yang, Y. Piao, H. Li, Y. Sun, Q. M. Xue, C. M. Xiong, R. F. Dou, and Q. Y. Tu, Appl. Phys. Lett. **93**, 173104 (2008).
[32]A. A. Mosquera, D. Horwat, A. Rashkovskiy, A. Kovalev, P. Miska, D. Wainstein, J. M. Abella, and J. L. Endrino, Sci. Rep. **3**, 1714 (2013).
[33]X. D. Li, T. P. Chen, P. Liu, Y. Liu, Z. Liu, and K. C. Leong, J. Appl. Phys. **115**, 103512 (2014).
[34]D. Pal, A. Mathur, A. Singh, J. Singhal, A. Sengupta, S. Dutta, S. Zollner, and S. Chattopadhyay, J. Vac. Sci. Technol. A **35**, 01B108 (2017).
[35]D. Pal, J. Singhal, A. Mathur, A. Singh, S. Dutta, S. Zollner, and S. Chattopadhyay, Appl. Surf. Sci. **421**, 341 (2016).
[36]H. Zaka, B. Parditka, Z. Erdélyi, H. E. Atyia, P. Sharma, and S. S. Fouad, Optik **203**, 163933 (2020).
[37]N. Ehrmann and R. Reineke-Koch, Thin Solid Films **519**, 1475 (2010).
[38]M. Mirzaee, A. Zendehnam, and S. Miri, Scientia Iranica F **20**, 1071 (2013), available at https://www.sciencedirect.com/science/article/pii/S1026309813000965.
[39]P. Wang, H. Du, S. Shen, M. Zhang, and B. Liu, Nanoscale Res. Lett. **7**, 176 (2012).
[40]T. E. Tiwald, J. A. Woollam, S. Zollner, J. Christiansen, R. B. Gregory, T. Wetteroth, S. R. Wilson, and A. R. Powell, Phys. Rev. B **60**, 11464 (1999).
[41]S. Zollner, P. P. Paradis, F. Abadizaman, and N. S. Samarasingha, J. Vac. Sci. Technol. B **37**, 012904 (2019).
[42]R. P. Lowndes, Phys. Rev. B **1**, 2754 (1970).
[43]A. Janotti and C. G. Van de Walle, Appl. Phys. Lett. **87**, 122102 (2005).

[44]S. Shokhovets, L. Spieß, and G. Gobsch, J. Appl. Phys. **107**, 023509 (2010).
[45]N. Ashkenov *et al.*, J. Appl. Phys. **93**, 126 (2003).
[46]H. Yoshikawa and S. Adachi, Jpn. J. Appl. Phys. **36**, 6237 (1997).
[47]G. E. Jellison and L. A. Boatner, Phys. Rev. B **58**, 3586 (1998).
[48]A. Schleife, C. Rödl, F. Fuchs, J. Furthm üller, and F. Bechstedt, Phys. Rev. B **80**, 035112 (2009).
[49]W. Y. Liang and A. D. Yoffe, Phys. Rev. Lett. **20**, 59 (1968).
[50]S. Shokhovets, G. Gobsch, and O. Ambacher, Superlattice Microst. **39**, 299 (2006).
[51]S. Shokhovets, O. Ambacher, B. K. Meyer, and G. Gobsch, Phys. Rev. B **78**, 035207 (2008).
[52]M. D. Neumann, C. Cobet, N. Esser, B. Laumer, T. A. Wassner, M. Eickhoff, M. Feneberg, and R. Goldhahn, J. Appl. Phys. **110**, 013520 (2011).
[53]M. Fox, *Optical Properties of Solids*, 2nd ed. (Oxford University, Oxford, 2010).
[54]J. S. Reparaz, L. R. Muniz, M. R. Wagner, A. R. Goñi, M. I. Alonso, A. Hoffman, and B. K. Meyer, Appl. Phys. Lett. **96**, 231906 (2010).
[55]W. T. Tsang and E. F. Schubert, Appl. Phys. Lett. **49**, 220 (1986).
[56]N. N. Syrbu, I. M. Tiginyanu, V. V. Zalamai, V. V. Ursaki, and E. V. Rusu, Physica B **353**, 111 (2004).
[57]D. R. Penn, Phys. Rev. **128**, 2093 (1962).
[58]N. M. Ravindra, S. Auluck, and V. K. Srivastava, Phys. Status Solidi B **93**, K155 (1979).
[59]S. Albrecht, L. Reining, R. Del Sole, and G. Onida, Phys. Rev. Lett. **80**, 4510 (1998).
[60]P. Gori, M. Rakel, C. Cobet, W. Richter, N. Esser, A. Hofmann, R. Del Sole, A. Cricenti, and O. Pulci, Phys. Rev. B **81**, 125207 (2010).
[61]D. J. Cirilo-Lombardo, Phil. Mag. **95**, 1007 (2015).
[62]J. B. You, X. W. Zhang, H. P. Song, J. Ying, Y. Guo, A. L. Yang, Z. G. Yin, N. F. Chen, and Q. S. Zhu, J. Appl. Phys. **106**, 043709 (2009).
[63]J. B. You, X. W. Zhang, S. G. Zhang, H. R. Tan, J. Ying, Z. G. Yin, Q. S. Zhu, and P. K. Chu, J. Appl. Phys. **107**, 083701 (2010).
[64]P. Y. Yu and M. Cardona, *Fundamentals of Semiconductors* (Springer, Heidelberg, 2010).
[65]S. Espinoza *et al.*, J. Vac. Sci. Technol. B **38**, 024005 (2020).
[66]C. Tanguy, Phys. Rev. Lett. **75**, 4090 (1995); *ibid.* **76**, 716 (1996).
[67]C. Tanguy, Phys. Rev. B **60**, 10660 (1999).
[68]H. Richter, Z. P. Wang, and L. Ley, Solid State Commun. **39**, 625 (1981).
[69]I. H. Campbell and P. M. Fauchet, Solid State Commun. **58**, 739 (1986).
[70]V. I. Korepanov, J. Raman Spectrosc. **2020**, 1 (2020).
[71]J. Serrano, F. J. Manjón, A. H. Romero, A. Ivanov, M. Cardona, R. Lauck, A. Besak, and M. Krisch, Phys. Rev. B **81**, 174304 (2010).
[72]M. Rajalakshmi, A. K. Arora, B. S. Bendre, and S. Mahamuni, J. Appl. Phys. **87**, 2445 (2000).
[73]K. A. Alim, V. A. Fonoberov, and A. A. Balandin, Appl. Phys. Lett. **86**, 053103 (2005).
[74]J. Humlíček, Phys. Status Sol. **215**, 155 (1999).
[75]See the supplementary material at: http://dx.doi.org/10.1116/6.0000184 for additional information regarding characterization of the ZnO layers using XRD, AFM, and XRR, ellipsometry results for bulk ZnO and quartz, and the determination of the band gap using a Tauc plot. It also contains a discussion of the errors in our ellipsometry analysis and a separation of the infrared dielectric function into several contributions.

Supplementary Material: Thickness dependence of infrared lattice absorption and excitonic absorption in ZnO layers on Si and SiO_2 grown by atomic layer deposition

(Dated: 19 April 2020)

Nuwanjula S. Samarasingha,[1] Stefan Zollner,[1] Dipayan Pal,[2] Rinki Singh,[3] Sudeshna Chattopadhyay [2,3,4]

[1)] *Department of Physics, New Mexico State University, P.O. Box 30001, Las Cruces, NM 88003, USA*

[2)] *Discipline of Physics, Indian Institute of Technology Indore, Indore 453552, India*

[3)] *Discipline of Metallurgy Engineering and Materials Science, Indian Institute of Technology Indore, Indore 453552, India*

[4)] *Discipline of Biosciences and Biomedical Engineering, Indian Institute of Technology Indore, Indore 453552, India*

S1. SURFACE ROUGHNESS

The surface roughness of our ZnO layers on Si and SiO_2 was determined by x-ray reflectance (XRR) and atomic force microscopy (AFM). Typical AFM and plan-view SEM images for similar layers are shown in Ref. 34. For the thickest ZnO layers on Si and SiO_2, the roughness was also studied with ellipsometry, by describing the surface roughness layer with the Bruggeman effective medium approximation (EMA) and a 50% void fraction.[19] Ellipsometry was not sensitive to surface roughness for thinner layers. AFM was performed on a Bruker Dimension FastScan instrument with a TESPA etched Si probe in non-contact tapping mode with a scan window size of 10×10 μm^2. The RMS surface roughness was calculated using the Bruker NanoScope analysis software and averaged over several sites. To compare the SE or XRR ellipsometry roughness with the AFM roughness, we must consider the unflattened AFM roughness, because the ellipsometry or XRR spot size is much larger than the AFM scan range.

A comparison of the roughness results for all three techniques is shown in Fig. S1: The surface roughness measured by XRR for the ZnO films on Si and SiO_2 substrates (see below) is in good agreement with the unflattened AFM RMS roughness.

Figures S1 (c) and (d) show the projections of the 3D AFM scans for the 51 nm and 5 nm ZnO/Si films, respectively, onto a plane perpendicular to the surface. The white frames, which identify the Bruggeman EMA layers, are about twice as high as the RMS surface roughness from AFM, because they extend from the lowest valley to the highest peak. We therefore show one half of the Bruggeman EMA layer thickness in Figs. S1(a) and (b), which compares well with the roughness determined from XRR and AFM.

TABLE SI. List of samples used in this study with nominal thickness t and results from XRR analysis, including thickness $t_{\rm XRR}$, interfacial SiO_2 layer thickness $t_{\rm SiO_2}$ (for ZnO on Si), surface roughness R from XRR, and average electron density ρ_e. For comparison, the bulk ZnO electron density is 1.51 e/Å^3. The layer thickness $t_{\rm SE}$ determined from ellipsometry is also given. The last two columns list the grain size d and the vertical strain $\epsilon_\perp$ measured with XRD.

Nominal t (nm)	Substrate	$t_{\rm XRR}$ (nm)	$t_{\rm SiO_2}$ (nm)	R (nm)	ρ_e (e/Å^3)	$t_{\rm SE}$ (nm)	d (nm)	$\epsilon_\perp$ (%)
5	Si	4.5	1.3	0.4	1.42	7.6	12	0.10
9	Si	9.5	1.4	0.8	1.44	11.2	12	0.47
19	Si	19.4	1.0	0.8	1.46	20.7	20	0.01
38	Si	36.0	1.5	1.6	1.50	37.2	27	0.07
52	Si	50.5	1.0	1.7	1.49	50.5	26	0.01
69	Si	69.1	1.4	2.0	1.48	NA	30	0.03
5	SiO_2	4.1	NA	1.1	1.35	4.1	NA	NA
9	SiO_2	8.7	NA	1.2	1.39	7.8	12	−0.19
19	SiO_2	18.8	NA	1.4	1.47	19.6	21	0.17
38	SiO_2	36.0	NA	1.7	1.49	34.1	31	0.10
52	SiO_2	51.5	NA	1.5	1.45	48.4(f)	31	−0.10
69	SiO_2	70.8	NA	1.1	1.44	NA	31	−0.05

S2. CRYSTAL STRUCTURE

The crystal structure of ZnO layers on Si and SiO_2 was investigated using x-ray powder diffraction on a PANalytical Empyrean diffractometer operated in line focus mode with 45 kV anode voltage and a 40 mA beam current producing Cu K_α radiation with λ=1.5419 Å wavelength. The bremsstrahlung continuum was removed using a Bragg-Brentano HD (BBHD) optical module with a fixed $\frac{1}{4}^\circ$ divergence slit, a 4 mm beam mask, 0.04 rad soller slits, and a fixed 1° anti-scatter slit as the incident beam optics. As the diffracted beam optics, we used a programmable anti-scatter slit, 0.04 rad soller slits, and a 0.02 mm thick Ni filter (to block the K_β radiation). The diffracted intensity was measured with a PIXcel1D-Medipix3 array detector (PANalytical).

Typical symmetric 2θ-ω scans of ZnO on Si and SiO_2 with different film thicknesses are displayed in Fig. S2. The XRD peaks were labeled according to the International Center for Diffraction Data database (PDF card number 01-079-2205). Since the ZnO (002) peak is the strongest, the layers have a preferred c-axis orientation, but other ZnO (100) and (101) peaks are also seen, especially in thicker layers. This indicates that the c-axis orientation is rather weak. For low-temperature growth of intrinsic (undoped) ZnO by ALD, both the polar (001)

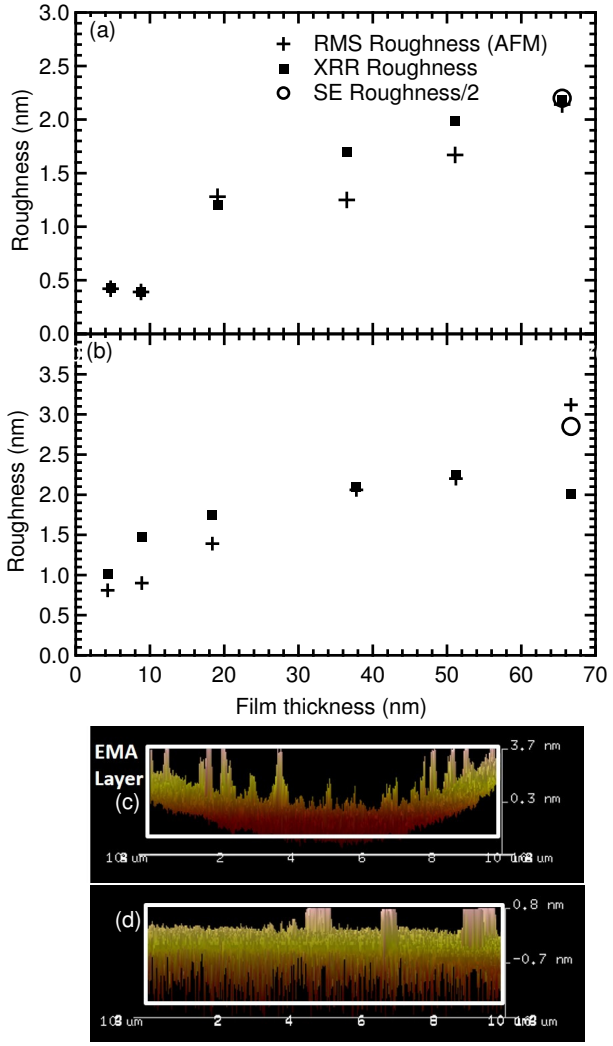

FIG. S1. Surface roughness of ZnO films on (a) Si and (b) quartz as a function of ZnO thickness. + and ■: unflattened root mean square (RMS) roughness determined from AFM and XRR, respectively; ◯: half of the roughness layer thickness obtained from an ellipsometry (SE) model with roughness. (c) Projection of the 3D AFM image for the 51 nm thick ZnO/Si film onto a plane perpendicular to the surface. The white frame shows the EMA surface roughness layer used to model SE data. (d) Same as (c), but for a 5 nm ZnO/Si layer.

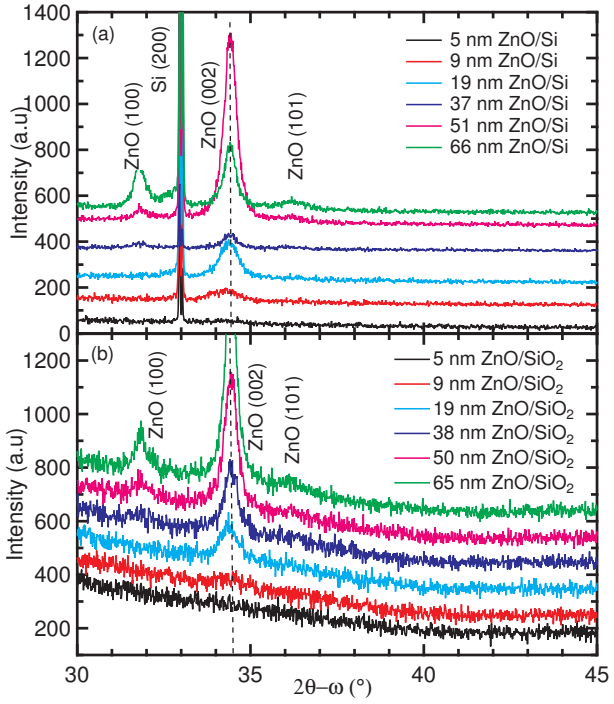

FIG. S2. X-Ray diffraction pattern for (a) ZnO/Si and (b) ZnO/SiO_2 with different film thickness.

and the charge-neutral (100) surface are expected,[28] consistent with the strongest XRD peaks in Fig. S2. The thinnest (5 nm) layers have barely visible x-ray diffraction peaks. They are either amorphous or there is insufficient scattering volume for diffraction using our experimental conditions. Similar XRD spectra were found for other ZnO layers produced by ALD[28,34] or magnetron sputtering.[30]

The grain height of polycrystalline thin films can be determined using the Scherrer formula (B. D. Cullity and S. R. Stock, *Elements of X-Ray Diffraction*, Prentice Hall, Upper Saddle River, NJ, 2001; P. F. Fewster, *X-Ray Scattering from Semiconductors and other Materials*, World Scientific, Singapore, 2015)

$$d = \frac{0.9\lambda}{\beta \cos\theta_B}, \tag{S1}$$

where β is the full width at half maximum (FWHM) of the Bragg peak (plotted as a function of 2θ, after subtracting the instrumental broadening) and θ_B the Bragg angle of the ZnO (002) diffraction peak. This grain size is often associated with the film thickness,[30,33] but this approach does not seem to work for our layers. For our thinnest (5 nm) layers, the grain height is 12 nm (which is not physically possible), see Table SI. For the thicker layers (38 to 69 nm thickness from XRR), the grain height is found to be around 31 nm, much less than the thickness. This discrepancy is not caused by the resolution of the instrument, since the FWHM of the Si (111) peak at 2θ=28.42° is only 0.11°, considerably less than the FWHM of the ZnO layer peaks. We conclude that our ZnO layers are very smooth, but have rather small grains, since they were grown at low temperature (200°C) and not annealed after growth.

From the position of the ZnO (002) peak in comparison with a bulk wurtzite ZnO crystal, we can determine the vertical lattice strain $\epsilon_\perp$, also given in Table SI. For all but one layer, the strain is small and not even the sign of the strain can be determined with certainty. Therefore, the variations of the dielectric function reported in this paper are more likely to be a function of thickness rather

than a function of strain, which has been reported from some piezo-electric materials, such as perovskites.[13–15]

S3. X-RAY REFLECTIVITY (XRR)

X-ray reflectance was used to obtain the ZnO layer thickness, electron density, and surface and interface roughness, with results given in Table SI. Data were taken on a PANalytical Empyrean instrument (same as for XRD) with a Ge (220) two-bounce hybrid monochromator, a fixed 1/32° divergence slit, and a 4 mm beam mask to produce a parallel beam. The reflected beam path consisted of a 0.27° parallel-plate collimator with a 0.1 mm XRR slit, a 0.04 rad soller slit, and a Xe proportional detector. A programmable beam attenuator with a 0.125 mm Ni foil was activated when the Xe detector count rate exceeded a preset threshold. The sample was aligned carefully to be perpendicular to the plane of incidence and to reduce the straight-through beam intensity by 50% at zero incidence angle.

XRR spectra for all samples, displayed as reflectance versus scattering vector

$$Q = \frac{4\pi}{\lambda}\sin\theta, \tag{S2}$$

where λ=1.5406 Å is the Cu $K_{\alpha 1}$ wavelength and θ the angle of incidence (measured relative to the sample surface), are shown in Fig. S3 on a semi-logarithmic scale. The data were analyzed using the Parrat formalism (L. G. Parrat, *Surface studies of solids by total reflection of x-rays*, Phys. Rev. **95**, 359, 1954) with details in Ref. 34, resulting in the sample parameters in Table SI. We used the MotoFit program (`http://motofit.sourceforge.net`) in an Igor Pro (Wavemetrics, Inc., Lake Oswego, OR, USA) environment to fit our XRR data and determine the fit parameters. For some samples, two or three ZnO layer sections with different electron densities were required to achieve a good fit between model and data. In such cases, the thickness given in Table SI is the sum of the individual thicknesses and the electron density is a weighted average over all ZnO sections.

Some trends are apparent by direct inspection of the XRR graphs. (1) The critical angle given by the sharp drop of the reflectance is nearly the same for all but the thinnest samples, indicating a nearly constant electron density (independent of layer thickness). (2) The period of the Kiessig fringes shows significant changes with layer thickness. (3) The agreement between data and fit is excellent using our model, indicating a high level of confidence in the accuracy of our layer thicknesses and densities. (4) The amplitude of the Kiessig fringes, which depends on the contrast of the electron density of layer and substrate, is nearly the same for ZnO on Si and on SiO_2, because Si and its oxide have nearly the same electron density. (5) The drop of reflectance versus Q is relatively slow, which allows us to measure reflectance

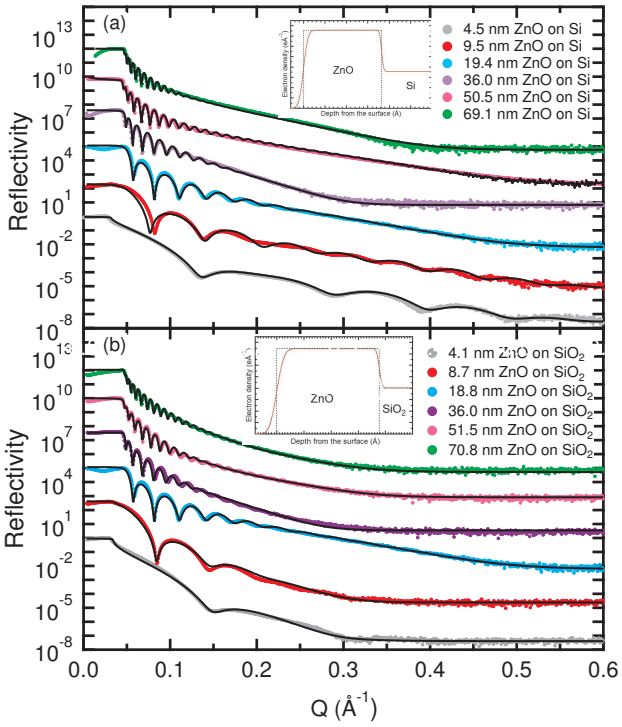

FIG. S3. X-ray reflectivity for (a) ZnO/Si with film thickness 5 nm, 9 nm, 19 nm, 37 nm, 51 nm, and 66 nm (b) ZnO/SiO_2 with film thickness 5 nm, 9 nm, 19 nm, 38 nm, 50 nm, and 65 nm. The solid line shows the model data and circles represent the experimental data. The curves were shifted vertically for clarity. The inset shows the electron density versus depth from the x-ray reflectivity fit for one thickness (38 nm).

for large values of Q. This indicates that the surface roughness for our ZnO layers is rather small.

Errors of the XRR thicknesses in Table SI can be estimated by manual variation of the parameters followed by visual comparison of the fit and the data ("chi-by-eye"). We found that the accuracy of the XRR thicknesses in Table SI was about 1%. The genetic algorithm is usually best suited for fitting XRR and high-resolution x-ray diffraction data to a model. Unfortunately, the Motofit implementation of this algorithm does not return any errors. We also tried fitting our data with a Marquardt-Levenberg algorithm in Motofit (which is said to return errors), but this algorithm did not converge for our data.

S4. OPTICAL PROPERTIES OF BULK ZNO

For comparison with results from thin ZnO layers on Si and SiO_2, we also performed ellipsometry measurements on a bulk c-axis oriented ZnO crystal obtained commercially. This work was described previously.[41] In summary, the ordinary and extraordinary dielectric func-

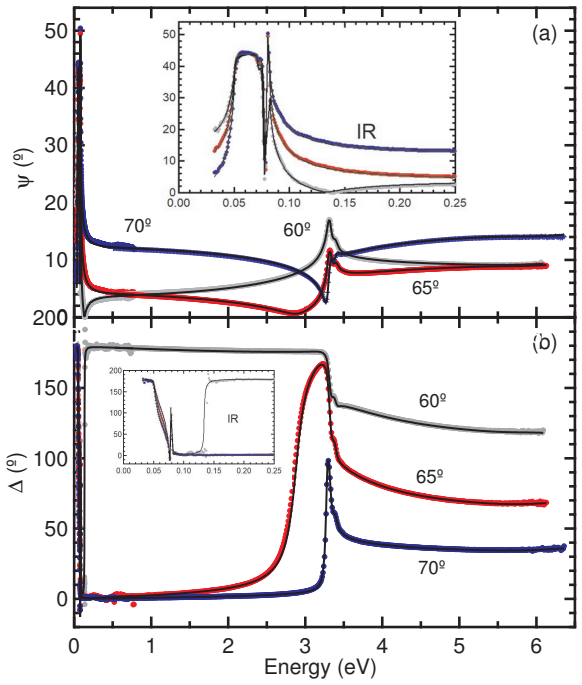

FIG. S4. Ellipsometric angles (a) ψ and (b) Δ for bulk ZnO with 21 Å surface roughness, similar to Ref. 41. Symbols: experimental data; solid: fit using Eq. (S3).

tion of wurtzite ZnO are each described as a product[41]

$$\epsilon(\omega) = \epsilon_{\mathrm{TO}}(\omega)\,\epsilon_{\mathrm{electronic}}(\omega), \tag{S3}$$

where the first factor[41]

$$\epsilon_{\mathrm{TO}}(\omega) = \frac{\omega_{\mathrm{LO}}^2 - \omega^2 - i\gamma_{\mathrm{LO}}\omega}{\omega_{\mathrm{TO}}^2 - \omega^2 - i\gamma_{\mathrm{TO}}\omega} \tag{S4}$$

describes the infrared lattice absorption and the second factor

$$\epsilon_{\mathrm{electronic}}(\omega) = 1 + \sum_i g_i(\omega) \tag{S5}$$

the optical properties due to interband transitions. ω_{TO} and ω_{LO} are the angular frequencies of the transverse (TO) and longitudinal (LO) optical phonons and γ_{TO} and γ_{LO} the corresponding broadenings. The terms $g_i(\omega)$ are called *oscillators*. They describe the electronic contributions to the dielectric susceptibility due to different types of interband transitions. For bulk ZnO, we used two Tauc-Lorentz oscillators with a common band gap in the near-gap region, one for the unresolved exciton triplet and another one for exciton-phonon complexes.[49–52] (N. O. Lipari, *Exciton energy levels in wurtzite-type crystals*, Phys. Rev. B **4**, 4535, 1971; B. Gil, *Oscillator strengths of A, B, and C excitons in ZnO films*, Phys. Rev. B **64**, 201310, 2001). At higher energies, we added two simplified Herzinger-Johs oscillators and a pole at 11 eV. In the infrared spectral range, the anisotropy is addressed by assigning different values to the phonon parameters for the ordinary and extraordinary beam. The sensitivity to the anisotropy is reduced in the visible and UV range for our experimental geometry. We therefore assume that the extraordinary part of the dielectric susceptibility is larger by 0.08 than the ordinary part throughout that spectral range. We call this a *partially anisotropic model*, because the anisotropy is included only in the infrared region and for ϵ_∞. This ignores the dichroism of ZnO.[44] Surface roughness was included within the Bruggeman effective medium approximation.

Figure S4 shows the ellipsometric angles ψ and Δ from 60° to 70° angle of incidence for bulk c-axis oriented ZnO from 0.03 to 6.5 eV obtained using FTIR ellipsometry and variable angle UV/VIS spectroscopic ellipsometry. The fit shows a partially anisotropic model with Eq. (S3) including surface roughness. The signs of anisotropy[40] are most apparent near 80 meV. The TO and LO phonon parameters from this fit are given in Table I. With this model, we extracted the ordinary and extraordinary complex dielectric functions (ϵ_o and ϵ_e) of bulk ZnO versus photon energy from 0.03 to 6.50 eV, as shown in Fig. S5. Because of the assumptions of our partially anisotropic fit, ϵ_{2e}=ϵ_{2o} and ϵ_{1e}=ϵ_{1o}+0.08 in the visible and UV range. The differences between the ordinary (E_1 phonon) and extraordinary (A_1 phonon) infrared lattice absorption are clearly visible by a shift of the infrared absorption and dispersion peaks.

S5. DIELECTRIC FUNCTION OF QUARTZ SUBSTRATE

Fused (amorphous) quartz substrates were purchased from EL-CAT Inc., Ridgefield Park, NJ. They were specified as UV grade fused silica, 20 by 20 mm in size with 500 μm thickness, and single-side polished with an rms roughness of no more than 0.5 nm. No XRD peaks were seen, see Fig. S2, only a broad background typical for amorphous materials. (Compare Y. Deng, Y. L. Du, M. S. Zhang, J. H. Han, and Z. Yin, *Nonlinear optical properties in $SrTiO_3$ thin films by pulsed laser deposition*, Solid State Commun. **135**, 221, 2005, for XRD spectra of thick $SrTiO_3$ layers on fused quartz. Our amorphous quartz XRD background looks similar.)

The ellipsometric angles ψ and Δ for 50° to 80° angle of incidence from 0.03 to 6.0 eV are shown in Fig. S6. ψ decreases monotonically from 0.5 to 6.0 eV (for the larger incidence angles) due to the normal dispersion of quartz, whose dielectric constant increases from 2.06 to 2.49 over the same energy range. Δ is negative in this energy range (for the larger incidence angles). Its magnitude increases with photon energy. This indicates that there is a thin surface layer which has a larger dielectric constant than quartz.

In the visible and UV spectral range, we describe the optical constants of quartz with an isotropic Sellmeier

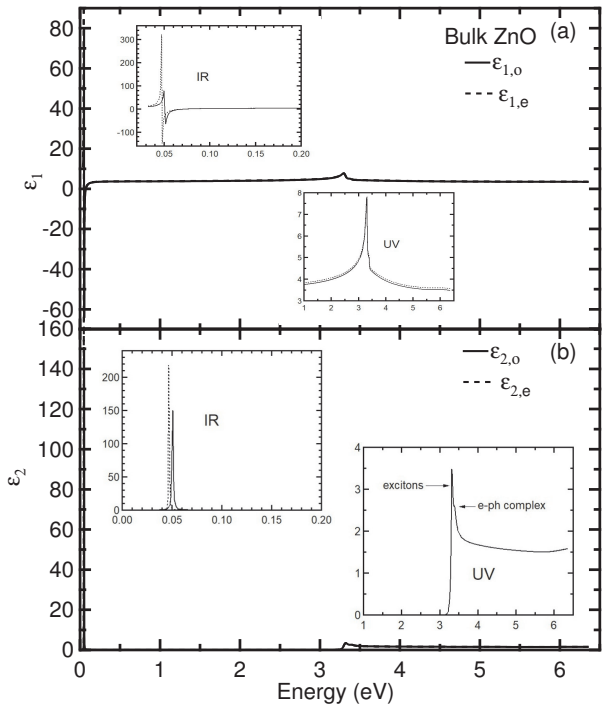

FIG. S5. (a) Real and (b) imaginary parts of the complex dielectric function for bulk ZnO versus photon energy, determined from the ellipsometric angles in Fig. S4 with a partially anisotropic model. Here ϵ_o and ϵ_e are the ordinary and extraordinary dielectric function, respectively

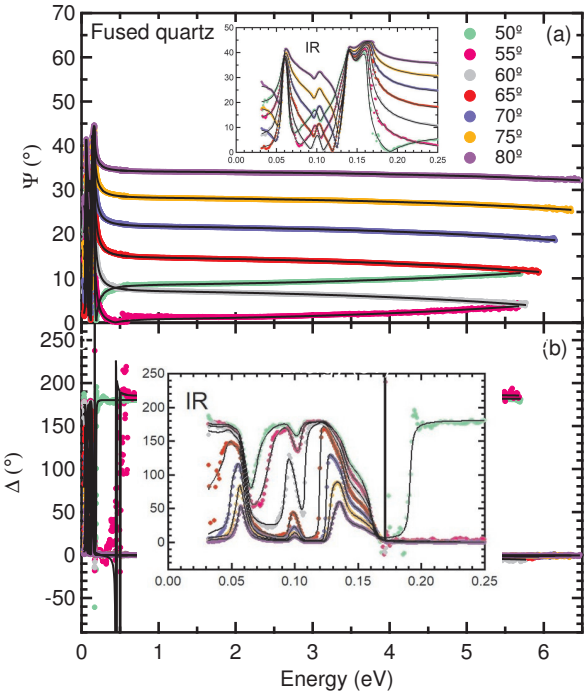

FIG. S6. Ellipsometric angles ψ and Δ for a bare single-side polished fused quartz substrate for angles of incidence from 50° to 80° (symbols). The lines show the best fit to a model which describes the quartz optical constants with a sum of Gaussians and poles and which includes a thin surface layer, which has a slightly larger ϵ than the substrate.

model, i.e., a constant value of ϵ_∞=1.24 and a pole at 11 eV (fixed) with a magnitude of 107 eV^2. (These parameters are strongly correlated and therefore have large errors. The pole energy is consistent with the band gap of quartz, often quoted between 9 and 10 eV.) For the surface layer, we assume the same parameters as for quartz, but with a larger value of ϵ_∞. The exact value of ϵ_∞ of the surface layer and its thickness are strongly correlated and cannot be determined separately. However, a surface layer thickness of 1 nm and ϵ_∞=1.76 for the surface layer achieve an excellent description of Δ in the UV region. (Adsorbed surface layers like water or oil usually have a smaller refractive index than glass and are not likely the reason for this surface layer. A SiO suboxide, on the other hand, has a larger refractive index than SiO_2 and might be a good candidate. There might also be polishing damage near the surface, for example residue from the slurry used for polishing, perhaps diamond or alumina, both of which have a larger refractive index than quartz. Surface characterization techniques such as Auger spectrometry or x-ray photoelectron spectroscopy were not available for our work.) In the infrared spectral region, absorption from molecular vibrations is described with a sum of eight Gaussians, taking the values established for thermal oxide as the starting point for our fit. The optical constants of the quartz substrate obtained from this model are shown in Fig. S7.

S6. COMPARISON OF OSCILLATOR AND POINT-BY-POINT FITS

After the oscillator fits using Eq. (1) were completed and the ZnO layer thicknesses on Si and SiO_2 determined, we also performed independent wavelength-by-wavelength (or point-by-point) fits, where the ZnO thickness was fixed and the real and imaginary parts of the dielectric function were treated as free parameters at each wavelength.[18,19] (Surface and interface layers were included in the point-by-point fit in the same manner as in the oscillator fit.) Both methods resulted in very similar dielectric functions (see Figs. S8 and S9), but the point-by-point fit is usually a little noisier than the oscillator fit. The agreement is usually better for ϵ_2 than for ϵ_1.

For ZnO on Si, we see a monotonic increase of ϵ_2 at 4 eV (above the band gap) from thinner to thicker films. The value of ϵ_2 below the band gap is very small. This indicates that our layered model is very good. Pseudo-absorption below the gap usually indicates that some of the layer thicknesses in the ellipsometry model are incorrect. For ZnO on SiO_2, ϵ_2 also increases from thinner to

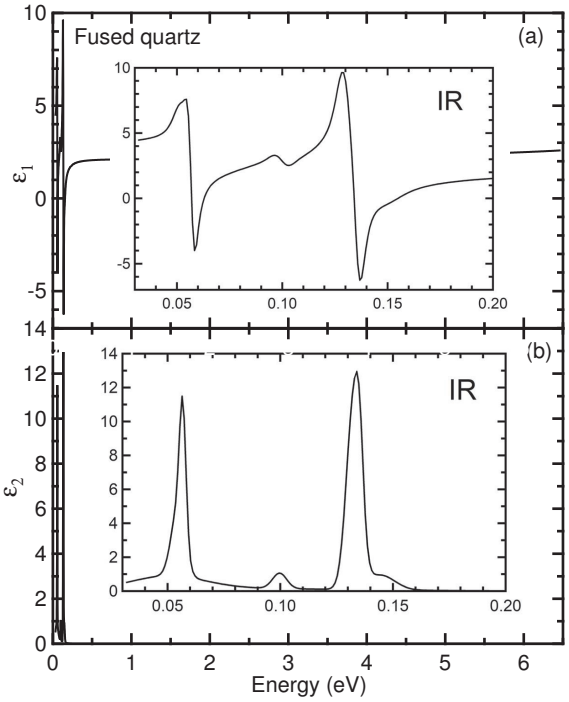

FIG. S7. Dielectric function of fused (amorphous) quartz, obtained by fitting the ellipsometric angles shown in Fig. S6. The insets show the infrared spectra region.

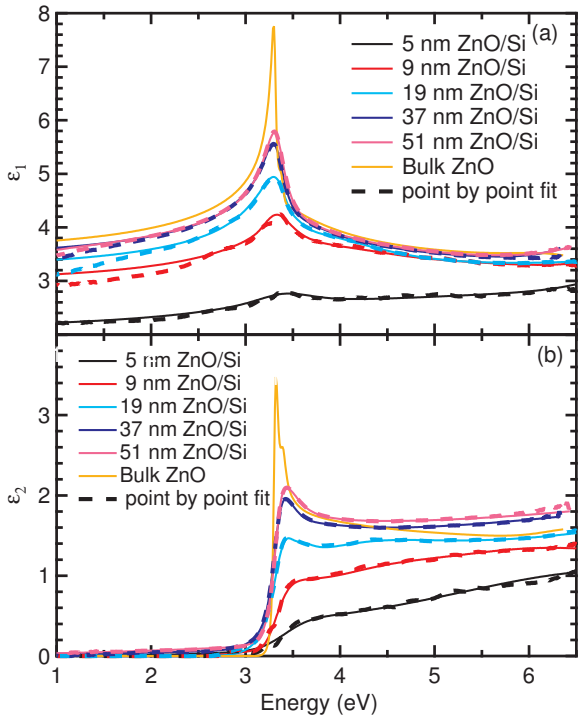

FIG. S8. Results from point-by-point fits to determine the optical constants of ZnO on Si for various thicknesses (dashed), in comparison to oscillator fits (solid). The mid-infrared spectral region is not shown, because the data are quite noisy in that range.

thicker films, but the increase is not entirely monotonic, because ϵ_2 at 4 eV is smaller for the 19 nm thick layer than for the 9 nm thick layer.

Small uncertainties in the optical constants of the quartz substrates can cause an apparent pseudo-absorption below the band gap. Therefore, it turned out to be crucial to develop accurate optical constants for our quartz substrates, see Sec. S5. In contrast to earlier work, there are no artifacts in the ϵ_2 optical constants near the band gap. ϵ_2 in ZnO thin layers qualitatively looks similar to the bulk, except that the exciton-phonon continuum is not resolved and the exciton peak is broader and weaker.

The agreement between the oscillator and point-by-point fit methods is also good for ϵ_1 near or above the band gap. For ZnO on Si, however, ϵ_1 from the point-by-point fit falls off faster towards the infrared than ϵ_1 from the oscillator fit. There is no physical reason for this faster dropoff, since there are no absorption processes between the TO phonon energy and the band gap. Therefore, we believe that the oscillator fit yields more accurate results for ϵ_1 than the point-by-point fit. The discrepancy for ZnO on Si might be due to inaccuracies in the treatment of the interfacial layer between the Si substrate and the ZnO layer or due to small errors in the optical constants of the Si substrate, see Sec. S10.

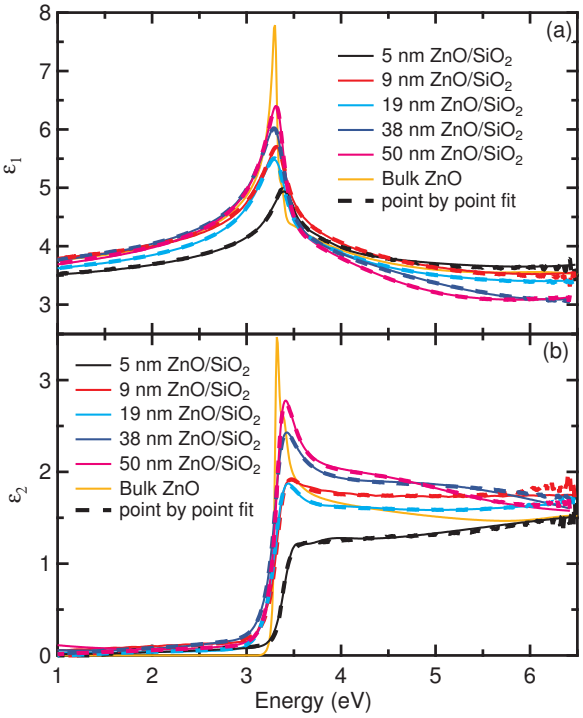

FIG. S9. As Fig. S8, but for ZnO on SiO_2.

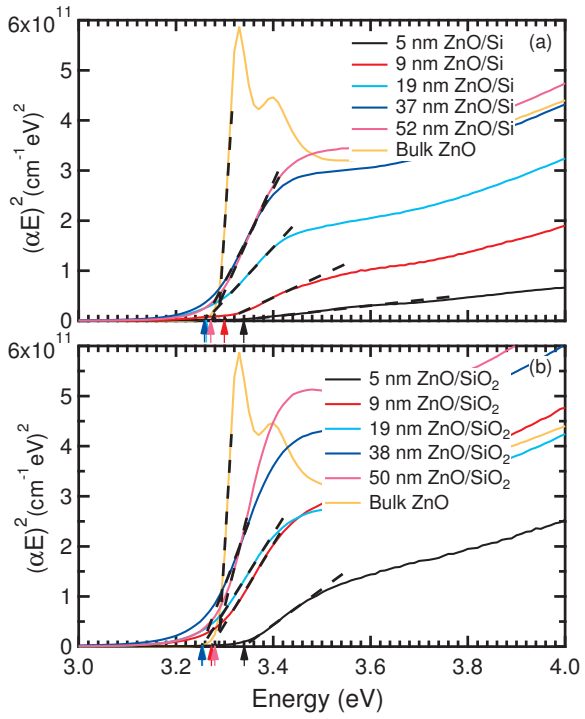

FIG. S10. Tauc plot extrapolation for bulk ZnO and (a) ZnO on Si (b) ZnO on SiO_2 with different film thickness

S7. BAND GAP DETERMINATION USING TAUC PLOT

The direct optical band gap of a material is often found by plotting $(\alpha E)^2$ versus E, where α is the absorption coefficient and E the photon energy. This is sometimes called a Tauc plot.[53] One looks for a linear region in this graph, extrapolates to zero, and then identifies the intercept with the optical band gap. While this technique is clearly arbitrary and influenced by the choice of the linear region and the extrapolation, it is used frequently. Figure S10 demonstrates the use of this technique to determine the band gap of bulk ZnO and thin ZnO layers on Si and SiO_2. When using this technique, it is very important to use the point-by-point optical constants (see Sec. S6) for the extrapolation, since the use of oscillators may bias the optical constants used for extrapolation. Results are shown and discussed in the main manuscript.

S8. COMPARISON OF ELLIPSOMETRY AND TRANSMISSION RESULTS

Some studies[31] report the absorption coefficient for thin ZnO layers determined using transmission measurements. This procedure is dangerous, because both the real and imaginary parts of the dielectric function (and complex refractive index) change with layer thickness, see Fig. 6, but only one quantity (transmitted intensity) is measured. One measured quantity cannot be used to determine two unknowns. Therefore, it is our position that transmission measurements by themselves cannot be used to determine absorption coefficients of a thin layer, unless the refractive index of the layer is well known (and does not depend on the deposition conditions of the layer).

On the other hand, it can be advantageous to combine ellipsometry measurements of a layer A on a single-side polished transparent substrate B with transmission measurements of the same layer A on a double-side polished substrate of material B. Both ellipsometry and transmission results can be loaded into a multi-sample environment and fitted simultaneously. The ellipsometry results will be more accurate for large absorption coefficients, while the transmission results will be more accurate for small absorption coefficients. Combining both datasets will lead to more accurate optical constants over the complete spectral range. A nice application of this technique to GaN on sapphire has been presented by Yu *et al.* (G. Yu, G. Wang, H. Ishikawa, M. Umeno, T. Soga, T. Egawa, J. Watanabe, and T. Jimbo, *Optical properties of wurtzite structure GaN on sapphire around fundamental absorption edge (0.78-4.77 eV) by spectroscopic ellipsometry and the optical transmission method*, Appl. Phys. Lett. **70**, 3209 (1997)).

Unfortunately, we could not use this technique, because we did not have ZnO layers on two-side polished quartz substrates. As a work-around, we performed transmission measurements of ZnO layers on our single-side polished quartz substrates (see Table SI) with the single-side polished bare quartz substrate taken as the transmission background. These transmission results (referenced to the single-side polished quartz substrate) should be similar to transmission results of the same ZnO layer on a double-side polished substrate (with a two-side polished quartz substrate as the reference). We therefore used these transmission results to determine the absorption coefficient (taking the refractive index from our ellipsometry measurements, see Fig. 6). The results are shown in Fig. S11 (dotted) in comparison to absorption coefficients determined from a point-by-point fit to ellipsometry results (solid). It can be seen that both datasets show the same trends (versus thickness and photon energy), but there is a constant offset, presumably due to artifacts from the scattering of the transmitted light by the rough back surface of the quartz substrate, which were not properly taken into account in our model. For this analysis, it is very important to consider the dependence of the refractive index on thickness (see Fig. 6). If that is neglected, then α shows the wrong trend versus thickness and pseudo-absorption artifacts appear below the band gap. We can also use the absorption coefficients determined from our transmission measurements to determine the band gap with a Tauc plot, see Sec. S7 and Fig. S10.

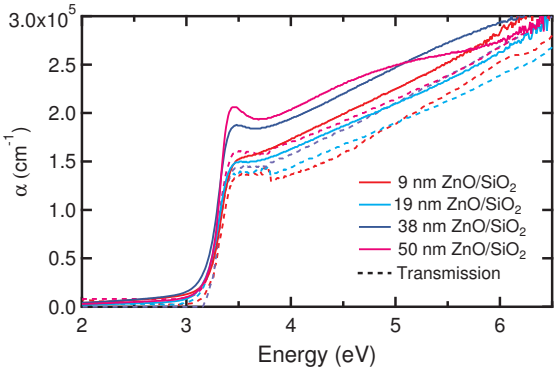

FIG. S11. Absorption coefficient of ZnO layers with different thicknesses on SiO_2 quartz substrates determined from ellipsometry measurements (solid) and transmission measurements of the same layers with the bare single-side polished quartz substrate as a reference (dotted).

S9. LATTICE VIBRATION VERSUS TOTAL INFRARED OPTICAL RESPONSE

As shown by Eq. (1), we write the total optical response as a product of three factors. The second factor describes the electronic contribution to the dielectric function. In the far-infrared region, this contribution is nearly constant and equal to

$$\epsilon_\infty = 1 + \sum_i g_i \left(\omega = 0\right), \tag{S6}$$

the high-frequency dielectric constant. One might also ask about the relative contribution of the E_1 infrared-active phonon to the total dielectric response in the infrared region. If we wrote the dielectric function as a sum of oscillators (which is the common method of treatment), then this question would be trivial to answer. As explained in Ref. 41, however, we have good reasons for our factorized approach. Most importantly, we want to fit our data while allowing two different broadening parameters for the TO and LO features from the E_1 phonon, but without an arbitrary parameter ϵ_∞, which comes from the second factor in our approach. Therefore, we attribute the quantity

$$\epsilon_{\mathrm{TOLO}}\left(\omega\right) = \epsilon_\infty \frac{\omega_{\mathrm{LO}}^2 - \omega^2 - i\gamma_{\mathrm{LO}}\omega}{\omega_{\mathrm{TO}}^2 - \omega^2 - i\gamma_{\mathrm{TO}}\omega} \tag{S7}$$

to the lattice contribution contained in the total infrared response. This quantity gets multiplied by the third factor (involving Gaussians) to obtain the total infrared optical response. Figure S12 shows the total dielectric function in the infrared region (solid) in comparison with the contribution from the E_1 phonon given by Eq. (S7) (dotted) for those layers where Gaussian oscillators where included in our model, see Tables I and II.

For ZnO layers on SiO_2, this decomposition looks as expected: The TO/LO absorption is lower than the total absorption. The Gaussian oscillators add absorption

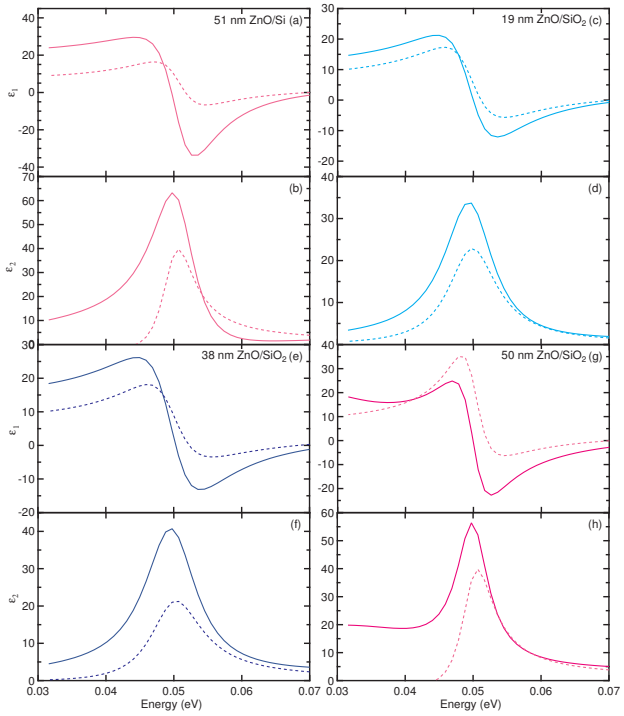

FIG. S12. Total dielectric function in the infrared region (solid) in comparison with the contribution from the E_1 phonon given by Eq. (S7) (dotted).

at very low energies and they also magnify the TO/LO absorption. The TO/LO absorption approaches the total absorption at high energies. Similarly, ϵ_1 is larger at low energies if the Gaussian absorption is included in the dielectric function and it magnifies the maxima and minima in the region of anomalous dispersion, but the Gaussian absorption makes little difference to ϵ_1 at the higher energies. For the 51 nm layer of ZnO on Si, the Gaussian contribution is larger (no longer a small correction) and therefore distorts the entire TO/LO lineshape, making it very asymmetric.

S10. IMPACT OF SI SUBSTRATE OPTICAL CONSTANTS

Several sets of optical constants for Si have appeared in the literature over the past 40 years, see Fig. S13. The silicon optical constants determined by Herzinger *et al.*[1] (often described as "Woollam silicon") are used nearly universally at universities as well as in the semiconductor industry to describe the optical response of dielectric layers on Si (001) substrates. Therefore, this dataset for Si was also the basis for our work. It is interesting, however, to ask how other optical datasets for the Si substrate optical constants will affect our results for the thickness-dependent dielectric functions of ZnO layers on Si. (For quartz substrates, as discussed in Sec. S5, we found it very important to develop our own opti-

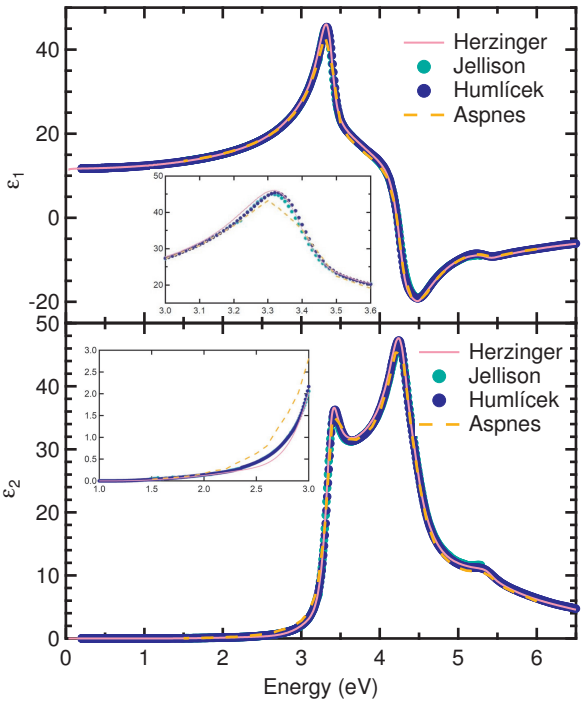

FIG. S13. Comparison of several sets of optical constants for the Si substrate referenced in the text.

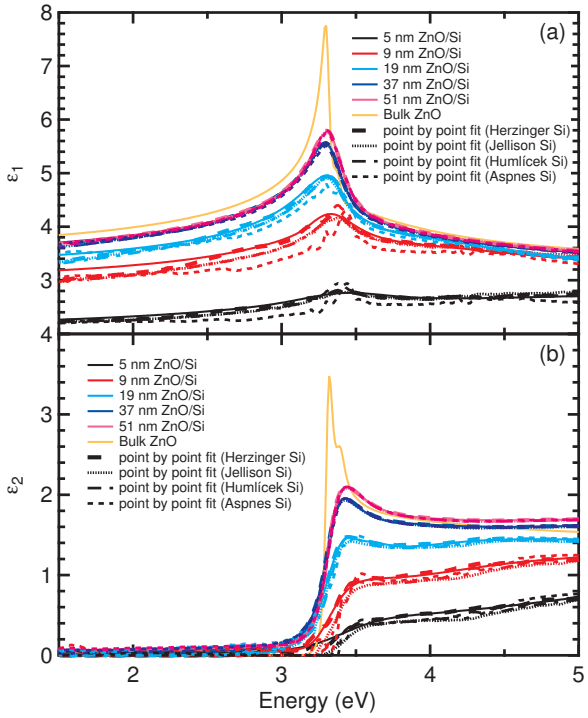

FIG. S14. Dielectric functions for ZnO layers on Si with different thicknesses as shown in Fig. S8, but with different reference constants for the Si substrate.

cal constants from a bare reference substrate rather than use optical constants from a database.)

The oldest comprehensive dataset for the dielectric function of Si is based on work by Aspnes and Studna (D. E. Aspnes and A. A. Studna, *Dielectric functions and optical parameters of Si, Ge, GaP, GaAs, GaSb, InP, InAs, and InSb from 1.5 to 6.5 eV*, Phys. Rev. B **27**, 985-1009 (1983)). This work was later revisited by Yasuda and Aspnes (T. Yasuda and D. E. Aspnes, *Optical-standard surfaces of single-crystal silicon for calibrating ellipsometers and reflectometers*, Appl. Opt. **33**, 7435-7438 (1994)). For three reasons, we did not select these datasets as Si reference constants for our work. (1) Aspnes often states that semiconductor optical constants depend on the surface orientation. These two papers cited above describe work performed on bare Si (111) surfaces, while our layers were grown on Si (001). (2) These data were taken on a rotating-analyzer ellipsometer without compensator. Therefore, the accuracy of these data for small values of ϵ_2 below 3.5 eV is limited. (3) These authors tried to minimize the thickness of surface overlayers to achieve a bare Si (111) surface. Since the dielectric function depends not only on the surface orientation, but also on surface conditions (M. K. Kelly, S. Zollner, and M. Cardona, *Modelling the optical response of surfaces measured by spectroscopic ellipsometry*, Surf. Sci. **285**, 282-294 (1993)), the Woollam Si data seem more appropriate to describe the dielectric function of a Si (001) substrate covered with transparent layers. The modern value of the early work by Aspnes *et al.* consists mainly in the precise description of preparing bare Si (111) surfaces.

Jellison (G. E. Jellison, *Optical functions of silicon determined by two-channel polarization modulation ellipsometry*, Opt. Mater. **1**, 41-47 (1992)) derived the silicon optical constants from a Si (001) surface with a phase-modulation ellipsometer, which provides accurate values of ϵ_2 below 3.5 eV. He also corrected his data for a thin oxide overlayer. Therefore, this data set is very accurate. Finally, Humlíček and Šik (J. Humlíček and J. Šik, *Optical functions of silicon from reflectance and ellipsometry on silicon-on-insulator and homoepitaxial samples*, J. Appl. Phys. **118**, 195706 (2015)) achieved very high accuracy of the Si (001) dielectric function below 3.5 eV with measurements of variable-thickness silicon-on-insulator substrates produced by wafer bonding and back etching of the donor wafer.

Four of these five sets of Si optical constants mentioned above are compared in Fig. S13. (We did not find a digitized set of the data by Yasuda and Aspnes.) More detailed comparisons were shown by Humlíček and Šik (2015). The overall agreement is excellent, but small differences exist, especially near the E_1 and E_2 critical points. The extinction coefficient also varies below 3.5 eV between datasets.

Figure S14 shows the optical constants for all our ZnO layers on Si obtained with a point-by-point fit, but with

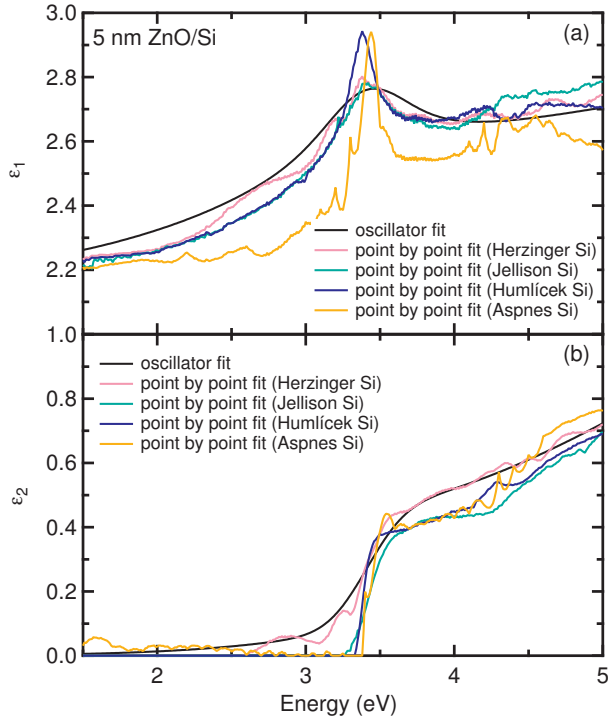

FIG. S15. As Fig. S14, but for the 5 nm ZnO on Si layer.

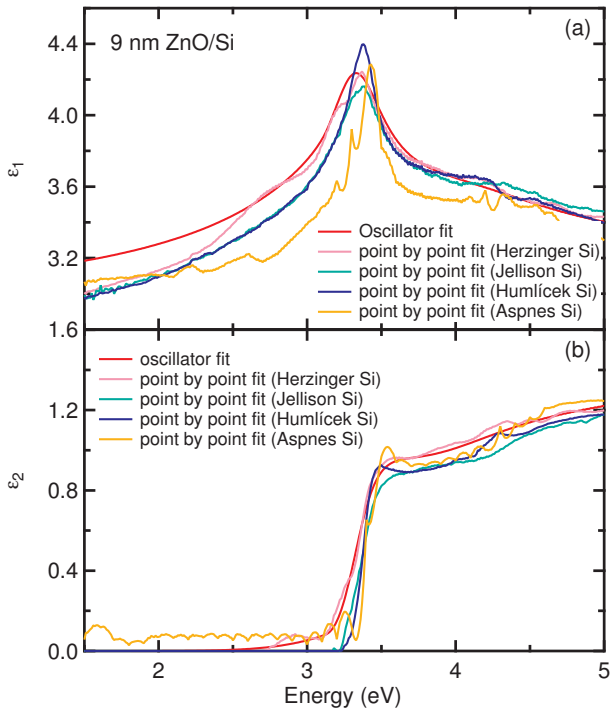

FIG. S16. As Fig. S14, but for the 9 nm ZnO on Si layer.

different Si substrate optical constants. The choice of the dielectric function of the Si substrate does not significantly influence the resulting ZnO optical constants for thicker layers, but differences are found for thinner ZnO layers, where the optical constants of the Si substrate have more influence. The largest differences can be seen for the Si optical constants of Aspnes and Studna (1983), which are probably the least accurate. Despite all these differences, the main conclusions of our work are not affected: There are significant monotonic variations of both ϵ_1 and ϵ_2 with ZnO layer thickness, which are not affected by the choice of the Si substrate optical constants.

Figures S15 and S16 show a magnified view of these comparisons for the thinnest ZnO on Si layers with 5 nm and 9 nm thickness. There are slight variations in the band gap given by the peak of ϵ_1 or the absorption threshold of ϵ_2 for different choices of the Si substrate optical constants. We also find different broadenings of the direct band gap given by the widths of the peak of ϵ_1 and the abruptness of the rise of ϵ_2. The choice of the Si substrate optical constants will have an influence on extracting exciton parameters (like exciton binding energy and broadening) for the thinnest ZnO layers. This will influence future work, when we consider excitonic effects and exciton-phonon coupling in our analysis.

S11. ACCURACY OF THICKNESSES DETERMINED FROM ELLIPSOMETRY

It is well known that spectroscopic ellipsometry cannot determine both thickness and refractive index for transparent layers as the thickness goes to zero.[18–20] For ultrathin layers, ellipsometry measures only the optical thickness, i.e., the product nt of the refractive index n and the thickness t. As the film thickness gets larger, interference fringes become visible, where the ellipsometric angle Δ jumps by 2π. The refractive index of the layer can then be determined from the amplitude of the interference fringes of the ellipsometric angle ψ, which is related to the optical contrast, i.e., the ratio of the refractive indices of layer and substrate. The spacing of the interference fringes is related to the optical thickness. The two quantities n and t can therefore be determined from the amplitude and spacing of the interference fringes. This method is implemented in commercial ellipsometry data analysis software.

In the intermediate thickness regime, one performs a uniqueness fit:[18] One fixes the thickness (over a certain range) and fits all other parameters, then plots the mean standard error from this fit versus thickness. If there is a clear minimum, then one can reasonably assume that the layer thickness is given by this minimum. We performed this procedure for our thinnest ZnO layer on Si, compare Table SI, where the XRR thickness (4.5 nm) deviates significantly from the ellipsometry thickness (7.6 nm). The result is shown in Fig. S17. We conclude from this

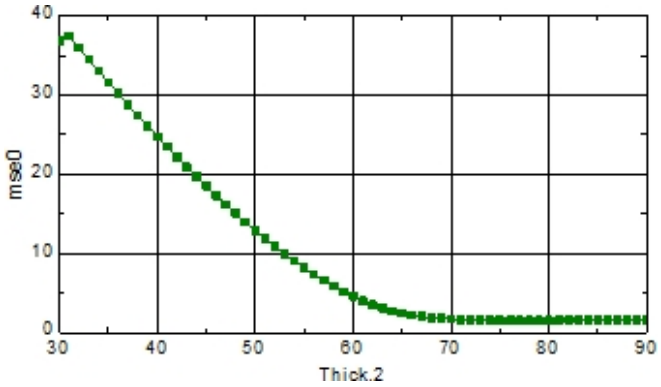

FIG. S17. Uniqueness fit (mean standard error versus thickness in Å) for a ZnO layer on Si with a nominal thickness of 5 nm.

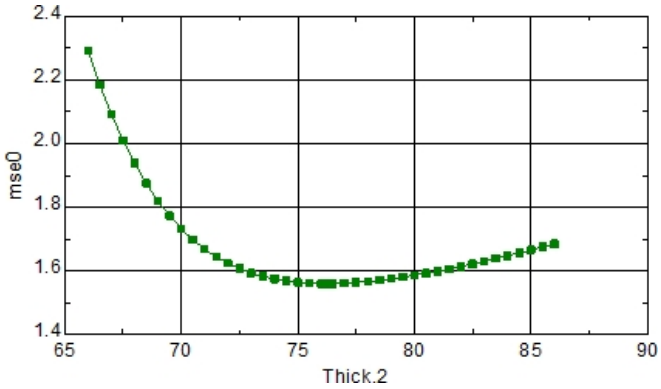

FIG. S18. Same data as in Fig. S17, but shown in a narrower range of thicknesses.

figure that the thickness of this layer is not at all likely to be less than 6 nm, but it might possibly be much thicker. We plot the same data in Fig. S18 on a narrower scale, which shows a clear minimum for t=7.6 nm. We conclude that the ellipsometry thickness of this layer is likely to be between 7.3 and 8.0 nm. (There are no generally accepted criteria in the ellipsometry community[18] on how to select a tolerance interval for a parameter from a uniqueness fit.)

We conclude that the roughly 50% difference of the thicknesses of the thinnest ZnO layer on Si determined from XRR and from ellipsometry (see Table SI) is much larger than the error of the XRR technique (about 1%, see Sec. S3) or the ellipsometry technique (about 5%, see above). How can we explain this? One of us has previously discussed the accuracy of several characterization techniques, especially XRR, ellipsometry, and transmission electron microscopy to determine the thickness of thin metal oxides on Si (S. Zollner, Y. Liang, R. B. Gregory, P. L. Fejes, D. Theodore, Z. Yu, D. H. Triyoso, J. Curless, and C. Tracy, *Limits of optical and x-ray metrology applied to thin gate dielectrics*, in *Characterization and Metrology for ULSI Technology 2005*, edited by D. G. Seiler, A. C. Diebold, R. McDonald, C. R. Ayre, R. P. Khosla, S. Zollner, and E. M. Secula, (American Institute of Physics, Melville, NY, 2005), AIP Conf. Proc. **788**, p. 166-171). As in this earlier work, we note that XRR considers an interfacial SiO_2 layer to be part of the Si substrate (because Si and SiO_2 have similar electron densities) while ellipsometry sees it as part of the layer (because ZnO and SiO_2 are much less polarizable than Si and have much smaller magnitudes of the dielectric function). We assumed a 1 nm thick SiO_2 interfacial oxide layer between Si and ZnO in our ellipsometry model, but it is possible that this interfacial oxide is thicker. Unfortunately, there is no good answer for the discrepancy between the XRR and ellipsometry results for the thickness of the thinnest ZnO layer on Si. This discrepancy for ZnO layers on Si becomes smaller as the layers become thicker. It is not a big issue for ZnO layers on quartz.

One might ask: What if the XRR thickness (4.5 nm) was the correct thickness of our thinnest ZnO layer on Si? What would the ZnO dielectric function be under this assumption? Unfortunately, we are not able to answer this question, because no good fit to the ellipsometric angles can be found while assuming a 4.5 nm ZnO thickness combined with a 1 nm thick SiO_2 interfacial layer. However, we are able to obtain a good fit if we assume a thickness of 5.0 nm for the thinnest ZnO layer on Si, combined with an interfacial SiO_2 layer thickness of 3.6 nm (rather than 1.0 nm as in our standard model described in Sec. III). The results from this fit are shown by the dashed lines in Fig. 5. Our main conclusions, a significant reduction of ϵ_1 below the band gap and a weakening of the excitonic absorption, are not affected qualitatively, but there are quantitative differences between the two models for the thinnest ZnO layer on Si.